Surface Acoustic Wave Longitudinally Coupled Resonators and Waveguide Coupled Resonators

by

Yufeng Xu, B.Sc., M.Sc.

A Thesis

Submitted to the School of Graduate Studies

in Partial Fulfilment of the Requirements

for the Degree

Doctor of Philosophy

McMaster University

July 1994

DOCTOR OF PHILOSOPHY (1994) McMaster University

(Electrical Engineering) Hamilton, Ontario

TITLE: **Surface Acoustic Wave Longitudinally Coupled Resonators and Waveguide Coupled Resonators**

AUTHOR: Yufeng Xu, B.Sc. (Ocean University of Qingdao, Qingdao, China)
M.Sc. (Academia Sinica, Beijing, China)

SUPERVISOR: Dr. Peter M. Smith

NUMBER OF PAGES: xii, 144

ABSTRACT

Surface acoustic wave (SAW) resonators, longitudinally coupled resonators and waveguide coupled resonators are studied in this thesis. The operation principles of these devices are examined. Standing wave pattern analyses are used in explaining the operation of the longitudinally coupled resonators. The coupling-of-modes (COM) theory is extensively used to characterize these devices. The COM theory is extended to the analysis of the coupled gratings and coupled transducers in which multi-track coupling is involved. The reflection, transduction and attenuation for the gratings and transducers are described in the COM model for these elements. Closed-form solutions of the COM equations for uniform structures are obtained. The matrix expression for these solutions, because of its modular nature, makes it very easy to cascade the different elements in a device and to analyze devices with different structures. The admittance matrix and scattering matrix can be calculated over the frequency range of interest. Efficient and accurate models are developed for these devices. There is good agreement between the simulated results and the experimental ones. The design procedure and optimization of waveguide coupled resonators are discussed and demonstrated. The longitudinal field distribution of the waveguide coupled resonator is calculated at the resonant frequencies of the devices. It is demonstrated that the extended COM theory can be used in the analysis of waveguide coupled resonators with more than two tracks. A four-track

waveguide coupled resonator is analyzed using the extended COM theory. Based on the understanding of the waveguide and longitudinally coupled resonators, a four-pole resonator with both longitudinal coupling and waveguide coupling is proposed and analyzed.

ACKNOWLEDGEMENTS

I would like express my deep appreciation to Dr. P.M. Smith for his active help, guidance, encouragement and support throughout this study. It is very difficult for me to express my thanks adequately. I would also express my thanks to Dr. C.K. Campbell for his guidance and concern in this study. I am also grateful for the guidance and counsel received from the other members of my supervisory committee, namely, Drs. T.D. Todd and P.E. Jessop. Special appreciation is extended to Dr. P.M. Smith for his time, invaluable comments and patience in reviewing this thesis.

I would also like to thank Mr. P.J. Edmonson for discussions and technical assistance in the experiment and Dr. S. Hassal for help in making some of the masks for the experiment.

I also like to thank my colleagues at Bell-Northern Research, namely, Drs. Z.H. Chen, J.D. Dai and J.C.B. Saw for helpful discussions during the writing of this thesis.

The financial support provided by the Department of Electrical and Computer Engineering in forms of scholarships, teaching assistantships and bursaries is grateful acknowledged.

I also wish to acknowledge the years of help and encouragement given to me by my parents. In addition, I wish to thank my wife for her encouragement, love, sacrifices and patience.

TABLE OF CONTENTS

LIST OF FIGURES

CHAPTER 1

INTRODUCTION

The behaviour of surface acoustic waves propagating on the surface of elastic solids has been known since last century when it was studied by Lord Rayleigh [1]. The existence of these surface acoustic waves was observed in earthquakes, and they were a subject in seismology. Since the invention of the interdigital transducer (IDT) in 1965 [2], the phenomenon of surface acoustic wave (SAW) propagation has been exploited extensively for applications in electronic circuits and great progress has been made in this field. Surface acoustic wave devices that perform sophisticated analog signal processing functions in electronic systems have been invented.

In this chapter, we will discuss the propagation of surface acoustic waves, the principles of SAW devices, and different structures of SAW resonators and coupled resonators.

1.1 Surface Acoustic Waves

The waves propagating on the surface of water in the ocean are a kind of surface wave. Similar surface waves can also propagate on the surface of elastic solid materials, in which case they are called surface acoustic waves.

When a surface acoustic wave propagates on the surface of a substrate, there is

movement of particles in the material. The amplitude of the wave decays exponentially with the substrate depth. For isotropic materials, the particle trajectory is elliptic [3].

The instantaneous displacement of particles of a surface acoustic wave propagating in an isotropic material is shown in Figure 1.1. The dots in this figure represent the equilibrium positions of the particles in the material, while the lines show the displacement when a surface acoustic wave is present. There is little motion at depths greater than one wavelength. The relative displacement is shown in Figure 1.2. Most of the energy associated with the surface acoustic wave is concentrated within one acoustic wavelength of the surface of the solid.

SAW devices are usually fabricated on piezoelectric materials which are anisotropic crystals or ceramics. The propagation of surface acoustic waves on these materials is more complicated than that on isotropic materials, but the basic properties of the surface acoustic waves are the same. The amplitude of the surface acoustic wave also decays with the substrate depth, with most of the acoustic energy concentrated within one wavelength from the surface.

The propagation velocity of the surface acoustic waves for a practical substrate is usually in the range of 2000 m/s to 5000 m/s, which is about 10^{-5} of that for electromagnetic waves in the air. Therefore the wavelength of the surface acoustic wave is about 10^{-5} of that for electromagnetic waves at the same frequency. Usually the size of the wave device is proportional to the wavelength of the waves. Thus, the dimensions of a SAW device are about 10^{-5} times those of electromagnetic wave devices operating

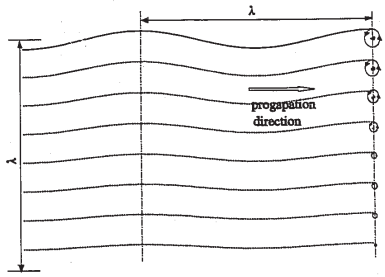

Figure 1.1 Instantaneous displacements for Rayleigh wave propagation in isotropic material.

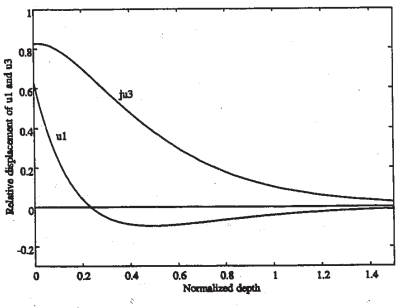

Figure 1.2 Rayleigh wave displacements in isotropic material. (u_1 is the displacement in the direction of propagation, u_3 is the displacement in the direction perpendicular to the surface)

at same frequency.

The operating frequency of SAW devices ranges from 30 MHz to several GHz. The low end of the range is limited by the size of the substrate, since at these low operating frequencies the devices become excessively large and costly. The upper operating frequency is limited by the lithographic resolution in the fabrication of the devices. The finger width is a quarter wavelength for standard IDTs and a higher frequency means a smaller wavelength. For example, a SAW device operating at 1 GHz requires the line width of about 1 μm. The highest reported operating frequency for a SAW device is about 17 GHz [4].

Since most of the energy in surface acoustic waves propagates on the surface of the substrate, these waves are easily excited, detected and perturbed by structures fabricated on the surface. Some common structures are the interdigital transducers, gratings and grooves. The interdigital transducer is a comb-like conductive structure deposited on the surface of a piezoelectric material that transforms electrical energy into acoustic energy, or vice versa. Gratings and grooves are used to produce reflections of waves in the device. These structures are implemented by a planar lithographic process similar to that used in the semiconductor industry. With these structures, sophisticated functions can be performed by SAW devices.

1.2 Surface Acoustic Wave Filters

To make use of the surface acoustic waves, they must be excited and detected as

desired. The interdigital transducer (IDT), invented in 1965 by White and Voltmer [2], is very efficient in the excitation and reception of surface acoustic waves on piezoelectric materials. The invention of the IDT opened a whole new field in analog signal processing devices.

SAW devices include filters, resonators, delay lines, matched filters, convolvers, etc. They can perform analog signal processing functions at a very high speed. A brief introduction to SAW filters is given to highlight the operation of SAW devices.

SAW devices are mostly built on the piezoelectric materials on which the surface acoustic waves are excited and detected by interdigital transducers. The most widely used SAW materials are lithium niobate ($LiNbO_3$), quartz, and lithium tantalate ($LiTaO_3$). The substrate is selected in consideration of the velocity, coupling coefficient, and temperature coefficient.

For a given centre frequency, a lower velocity requires a shorter finger period and consequently, leads to a smaller chip size. Greater velocity is desirable for high frequency devices in order to make the fabrication easier.

The coupling coefficient is an measure of transformation between the electric energy and the mechanical (SAW) energy. In a SAW transversal filter, the minimum insertion loss and the maximum relative bandwidth depend on the coupling coefficient. Generally, a wider bandwidth requires a larger coupling coefficient.

The frequency response for the SAW device will change with the ambient temperature. The major effect is a shift in the centre frequency. The temperature coefficient is a measure of the velocity sensitivity to temperature change. Filters with a

narrow bandwidth require a substrate with a small temperature coefficient. Although both high coupling and low temperature coefficients are desired, the ideal piezoelectric material has not yet been discovered. In choosing the substrate, all factors must be considered together, which usually results in tradeoffs among the different characteristics of the materials.

The simplest SAW device is a SAW delay line, which is shown in Figure 1.3. In this device, two unapodized interdigital transducers on a polished piezoelectric substrate, such as lithium niobate or quartz, are employed for the generation and reception of the surface acoustic waves. When an AC voltage is applied to the input IDT, elastic stresses will be produced because of the piezoelectric property of the substrate. The elastic stresses will propagate as surface acoustic waves on the substrate along the x-direction and will reach the output IDT after some delay. An inverse process occurs at the second IDT, where the acoustic waves are converted into electrical energy that is dissipated by the load.

At the input IDT, the fingers of the IDT can be viewed as independent line sources of acoustic pulses when subjected to an applied electrical impulse excitation. The acoustic pulses will travel in both the positive and negative x-directions on the substrate. If there were an ideal line receiver to transform the acoustic pulses into electric pulses, a train of electrical pulses would be obtained. The frequency response of the transducer

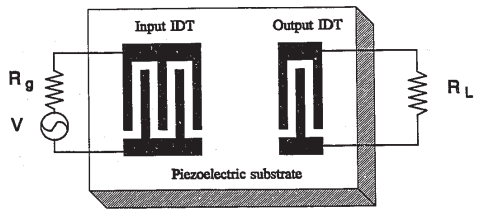

Figure 1.3 The simplest SAW device: SAW delay line

is the Fourier transform of this impulse response.

An inverse process can also be expected when an acoustic pulse generated by a line source propagates under an IDT. A train of electric pulses will be detected at the IDT electrodes. This behaviour illustrates the reciprocity principle in electro-acoustic transformation. The acoustic pulses generated by the IDT with applied electrical excitation or the electric pulses generated by the IDT with acoustic excitation are proportional to the finger length of the IDT. The IDT can be modeled as a transversal filter in which the delay between each tap corresponds to the acoustic delay of pulses and the weight of the tap is proportional to the corresponding finger length. This permits the design of IDTs with the use of design techniques developed for digital finite impulse response (FIR) filters. The process of varying finger lengths is called apodization, and an IDT with varied finger lengths is called an apodized IDT. Figure 1.4 gives an example of a SAW filter using an apodized IDT with an unapodized IDT.

The frequency response of SAW transversal filters can meet very stringent specifications using different apodization methods. These filters are widely used in television transmitters and receivers, satellite communication systems, and fiber optic communication systems. SAW transversal filters have demonstrated a very impressive capability to meet the demanding requirements of high-performance communication systems, such as the vestigial sideband filter in TV transmitters and the spectrum shaping filter in digital microwave radios [5].

Since the IDT is bidirectional, at least half of the energy generated by the IDT is lost without reaching the receiving IDT, leading to a minimum of 3 dB loss at the

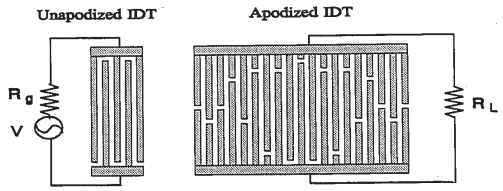

Figure 1.4 SAW filter with an apodized and an unapodized IDTs

transmitting IDT in a SAW filter. Reciprocally, the loss at the receiving IDT is also at least 3 dB. Therefore the minimum insertion loss for this type of filter is 6 dB.

Another problem with SAW transversal filters is the triple transient interference (TTI), which is caused by the regeneration of the surface acoustic waves by the input and output transducers. The TTI degrades the amplitude and phase response of the filter in the passband, but can be controlled by the matching conditions at the input and output transducers. Unfortunately, the IDTs matched for low insertion also exhibit large TTI. In practice, the transducers are often intentionally mismatched to reduce triple transit interference and, as a result, insertion losses in excess of 20 dB are common. These problems prohibit the application of transversal filters in the front-end of receivers.

To overcome the disadvantage of the high insertion loss of transversal filters, great efforts have been made in the development of the unidirectional transducers (UDT) [6,7,8,9,10,11]. The UDT only transmits the acoustic wave at one direction. Therefore the bidirectional loss with the conventional IDT is avoided. The SAW filters employing UDTs can be matched with low insertion loss and low TTI simultaneously. However, the filters using UDTs often need either complex external matching circuits and/or more complicated device structures. These requirements make it more difficult to produce these filters at high frequencies (e.g. radio frequency (RF) receiver at 900 MHz to 2 GHz for cellular phones).

SAW coupled resonators exhibit very low insertion loss with simple matching circuits. Their use of single finger IDTs makes them easier to fabricate for high frequencies (e.g. GHz range). As a result, coupled resonators are finding more

applications in RF receiver front-ends. Their low insertion loss character is also desirable for intermediate frequency (IF) applications.

1.3 Surface Acoustic Wave Resonators and Coupled Resonators

A SAW resonant cavity is formed between two grating arrays. Due to the complex mixture of the shear and longitudinal motions of surface acoustic waves, the full reflection of a wave cannot be achieved with a single abrupt discontinuity [12]. Instead, a distributed reflector is necessary to achieve good reflection. The reflector is formed by periodic discontinuities caused by metal strips or grooves. If the period of the metal strips or grooves is half a wavelength of the surface wave, the reflection from each finger will add in phase. A sufficiently long reflector array will result in a large reflection.

A one-pole SAW resonator can be formed by placing one or two interdigital transducers (IDTs) between two gratings. Typical structures and equivalent circuits for a one-port and a two-port SAW resonator are shown in Figure 1.5 and Figure 1.6 respectively. The two reflection gratings confine the acoustic energy near their Bragg frequency. The resonant frequency is determined by the distance between the gratings and the period of the reflection gratings.

SAW resonators are primarily used as high Q (~10^4) feedback elements for oscillators. Their very narrow bandwidth makes them of little use in filter applications. However, the bandwidth can be dramatically increased with the use of coupled-resonators. Since the energy is confined in the cavities, the energy loss in the resonators is very

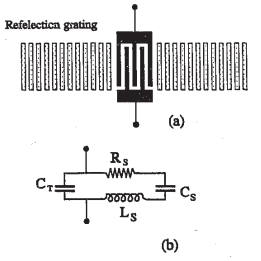

Figure 1.5 (a) One-port SAW resonator (b) lumped equivalent circuit

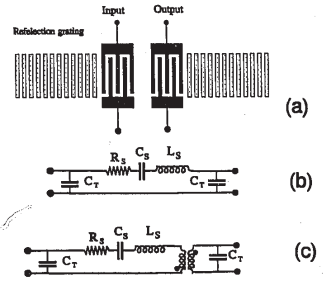

Figure 1.6 (a) Two-port SAW resonator. (b) lumped equivalent circuit for two-port resonator with no phase inversion. (c) with 180° phase inversion at resonance.

small, resulting in a very low insertion loss when the device is properly matched.

The coupling between resonators can be realized by a variety of coupling mechanisms, with IDTs, multistrip couplers, partially transmitting gratings, or waveguides [13, 14]. The simplest form of coupling is achieved by placing two one-port resonators in-line [13]. The structure of this device is shown in Figure 1.7(a). The two resonators share the reflector grating in the centre. The coupling can be controlled by the number of reflectors in the centre grating, which in turn determines the bandwidth of the resonator filter. This type of coupling has the advantages of preserving the natural resonator transverse mode shape and providing a large range of coupling strengths from very weak to very strong. Its significant drawback is that the out-of-band rejection is relatively poor because the centre grating is transparent to surface acoustic waves that are out of the stopband of the grating.

Another structure is the multistrip coupler coupled resonator [13] shown in Figure 1.7(b). In this structure, the two resonators are coupled transversely through the multistrip coupler. This type of coupled resonator offers possible enhancement of out-of-band rejection, but is not appropriate to be built on low electro-mechanical coupling substrates such as quartz [15].

Waveguide coupled (WGC) resonators and the longitudinally coupled resonators have found widespread use for a variety applications because of their superior electrical performances. The waveguide coupled resonators have very steep shape factors and impressive out-of-band rejections. They are practical for fractional bandwidths <~ 0.1 %. On the other hand, the longitudinally coupled resonators can provide a fractional

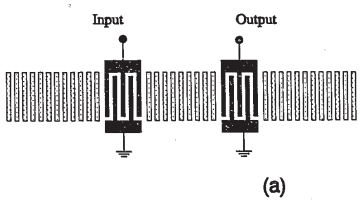

Figure 1.7 (a) SAW in-line coupled resonator

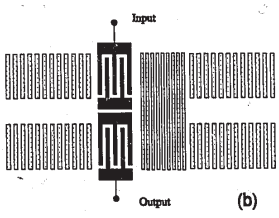

Figure 1.7(b) SAW coupled resonator using multistrip coupler

bandwidth as large as 7% on strong electro-mechanical coupling substrate. These two devices will be the focus of this thesis.

1.3.1 The Waveguide Coupled Resonators

The structure of a waveguide coupled resonator is shown in Figure 1.8. In this structure, the two resonators a placed in close proximity to each other. The coupling between the two resonators is caused by the evanescent energy distribution of each track.

The SAW waveguide coupled resonator was proposed by Tiersten *et al* in 1975 [16] and was later demonstrated experimentally [17,18]. In the early experimental devices, waveguides were formed by layers of MgO on quartz [18]. In 1984, Tanaka *et al* [19] did an analytical and experimental study on the device. The guiding effects of the metal gratings on the surface of the substrate (ST-quartz) were used to form the waveguides. By using the fundamental symmetric and anti-symmetric modes, a double mode coupled resonator was constructed. They studied the frequency splitting with the aid of waveguide models and demonstrated experimentally two-pole and four-pole resonators, the latter obtained by cascading two two-pole resonators. The waveguide coupled resonator was shown to have very good filter characteristics, such as bandwidth control and out-of-band rejection.

Subsequently, the study of this device has been pursued on two fronts. Hunt *et al* [20,21] did an experimental study on the transversal mode and longitudinal mode profiles using a laser probe and performed an analysis of the transverse mode profile using

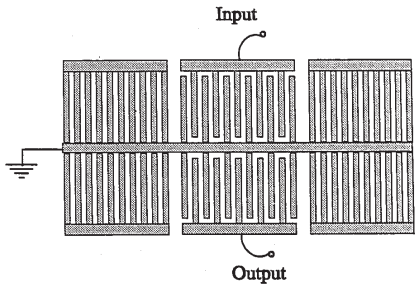

Figure 1.8 SAW waveguide coupled resonator

waveguide model. At the same time, the frequency response and its relation to the physical design of the device was being studied by others.

In modelling SAW resonators, coupling-of-modes (COM) theory [22,23] has been considered to be accurate and computationally efficient. The first attempt to use the approach for WGC resonators was made by C.K. Campbell *et al* [24] using the COM in time and COM in space approaches. Hartmann *et al* [25] later attacked the problem by assuming the coupled resonator as a combination of two one-pole resonators. The one-pole resonators were each modelled by using the COM theory. Then the admittance matrix of the coupled resonator was calculated with the help of a transformation to an equivalent circuit. The COM parameters for the device were obtained by experimental means [26].

The author proposed an alternative method by extending the COM theory to the coupled gratings and coupled transducers [27,28]. The previous COM theory for modelling SAW gratings and interdigital transducers (IDT) only considered one track. In the case of waveguide coupled resonators, two or more gratings and IDTs are coupled to produce multi-mode resonators [14,19,29]. The COM theory for the modelling of gratings needs to be extended to accommodate the coupling between the tracks. The resulting extended COM theory is more flexible.

1.3.2 Longitudinally Coupled Resonators

SAW coupled resonators usually have very narrow bandwidth due to their

resonator property. However, in 1992, Morita *et al* proposed the longitudinally coupled resonator filter with factional bandwidth as large as 7% built on large coupling materials. In this device, two longitudinal modes were supported in the cavity formed by the reflection gratings.

Figure 1.9 shows the structures of longitudinally coupled resonators. Generally, several resonant modes are possible within a cavity formed by two reflection gratings and can be used to realize multi-mode resonators. Usually, this is done by combining the first and second or the first and third resonant modes. On high coupling material, a flat passband can be produced between the two resonance frequencies. This type for resonator filter has fairly large bandwidth at the passband.

The structure of this device is very similar to that of the two-port resonator. In this case, the distance between the two IDTs is chosen to excite and detect the two resonant modes by the input and output IDTs, respectively. The advantage of this type of coupled resonator is that the frequency difference between the two modes can be quite large. On a material with a strong electro-mechanic coupling coefficient, the filter can have a large bandwidth, a flat passband, and very low insertion loss when matched. Since the input and output IDTs can 'see' each other, the out-of-band rejection is small. Larger out-of-band can be achieved by cascading two or three coupled resonators in tandem.

The longitudinally coupled resonator is an new device. Much work remains to be done to characterize the device.

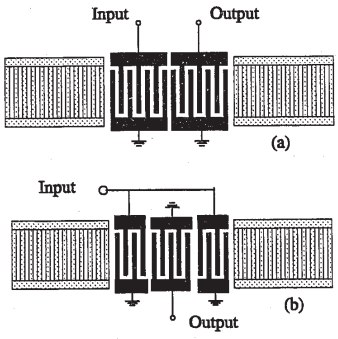

Figure 1.9 SAW longitudinally coupled resonator (a) using the first and second longitudinal modes. (b) using the first and third longitudinal modes.

1.4 Motivation of This Study

Progress in the communication industry has led to an increasing need for SAW filters which can meet the demanding requirements of high frequency, low insertion loss, desirable bandwidth, compactness, ruggedness, and low cost. SAW transversal filters have a large insertion loss caused by the bidirectional property of the interdigital transducers. This prohibits their use in receiver front-ends.

To acquire low insertion loss and reduce the triple transient interference, much effort has been targeted at the development of unidirectional transducers (UDT). So far, all techniques for creating unidirectional transducers have suffered from one drawback or another. Usually the unidirectional transducers require complicated phase shifting networks or lead to complicated electrode structures. This makes the fabrication more difficult for high frequency applications.

The longitudinally coupled resonators are fabricated on high electro-mechanic coupling coefficient material and have a large bandwidth and very low insertion loss. Because the filters employ quarter wavelength electrodes only, they are very suitable for high frequency applications such as the transmission and reception of wideband communications. The waveguide coupled resonators have narrow passband, low insertion losses, and high out-of-band rejections. They are good choices for narrow band applications.

Accurate modelling is necessary for the efficient design of the devices. The purpose of this study is to provide accurate models for the two different types of coupled

resonators. By using these models, the electrical properties of the devices can be predicted for given design parameters such as the layout, metal film thickness, and materials characteristics. The optimization in the design can be achieved by using the simulation iteratively. This can lead to the optimal performance of the devices.

The coupling-of modes theory will be used in the modelling of these devices. However, this theory is normally only used for the single track devices. In the waveguide coupled resonators, the gratings and transducers are coupled in parallel and there are two or more tracks in a device. In this case, the coupling of waves between different tracks must be included.

In this thesis, the COM theory is extended to account for such coupling. By use of the extended COM theory, the reflection, transduction and coupling of waves between different tracks can be described.

1.5 Scope of the Thesis

The objective of this thesis is to develop models for SAW coupled resonators and to verify the models by comparing the simulation results with the experimental ones.

Coupling-of-modes theory is used to model the coupled resonators. A major contribution of this work is that a COM theory is developed for coupled gratings and coupled transducers. The closed-form solution for uniform coupled gratings and transducers is obtained. Using this theory, the operation of the waveguide coupled resonator filter is described accurately.

Two computer programs are developed for the simulation of these two different devices. The Y-parameters of the coupled resonators are calculated based on this model, and the S-parameters can thereby be calculated. Based on the simulations, optimized coupled resonators are designed. Several devices are designed, fabricated and measured to verify the models. Experimental results agree well with the theoretical simulations.

This thesis is organized into five chapters. Chapter 2 deals with the coupling-of-modes theory and the solution of the coupling-of-modes equations. Chapter 3 discusses the modelling of the two-port resonators and of the longitudinally coupled resonators. The simulation and experimental results are compared. Chapter 4 presents the modelling of the waveguide coupled resonators and the experimental and simulation results. Finally, Chapter 5 will conclude the thesis.

CHAPTER 2

COUPLING-OF-MODES THEORY FOR SAW GRATINGS AND TRANSDUCERS

2.1 Introduction

The coupling-of-modes (COM) theory was developed to describe the phenomenon of coupling of waves in microwave tubes in the 1950's [30]. Since then, it has been used in analyzing a wide range of devices including holograms [31], distributed feedback lasers [32] and waveguide couplers in optoelectronics [33].

More recently, COM theory has been used to model SAW grating filters [34] and reflection gratings in SAW resonators [13]. In these analyses, the COM theory was applied to the passive elements, not to the interdigital transducer. Later, COM theory was applied to SAW interdigital transducers by adding a term to account for the transduction of surface acoustic waves [8]. Since then, COM theory has been widely used to analyze different types of SAW devices, such as resonators and single phase unidirectional transducers (SPUDTs). These devices require that the reflection and transduction of acoustic waves be considered simultaneously.

In all of the SAW devices mentioned above, the waves can be considered to be travelling along a single track. As a result, the COM equations are one dimensional, along

the travelling direction of the waves. With the coupling-of-modes descriptions and the device parameters, the electrical properties of a SAW device can be modelled accurately and efficiently.

In the case of waveguide-coupled resonators, coupling between the two resonators, due to the evanescent energy distribution of the modes in each of the two resonators, occurs in both the IDT and reflector regions. These gratings and transducers will hence be called coupled gratings and coupled transducers, respectively, to discriminate them from the single track versions.

In this chapter, the coupling of modes theory for single track structures will be reviewed. Then the COM theory for coupled multi-track structures will be developed. The extended COM theory for coupled gratings and coupled transducers will then be introduced. It will be shown to have good flexibility in describing an arbitrary arrangement of coupled reflection gratings and coupled interdigital transducers [27,28]. The closed-form solutions for the COM equations of uniformly coupled gratings and coupled transducers are given. These solutions is derived in the appendix.

2.2 COM Theory for SAW Reflection Gratings

In SAW devices, metal gratings or grooves are used for the reflection of acoustic waves. A grating is an array of metal strips or grooves made on the surface of the substrate by a lithographic process. The discontinuities produced by the strips or grooves cause reflections of waves. If the period of the grating is an integer number of half

wavelengths, the reflected waves from each strip will add in phase. While the reflection at each strip or groove may be very small, strong reflection may result near the Bragg frequency for a long array. Although the reflection occurs at the edges of the strips, they can be treated as a distributed reflection since the distance between the strips is very small.

Consider the periodic grating shown in Figure 2.1. The period of the grating is Λ. We define the waves travelling in each direction as

$$W^+ = w^+(x)e^{-j\frac{\pi}{\Lambda}x}$$
$$W^- = w^-(x)e^{+j\frac{\pi}{\Lambda}x} \qquad (2.1)$$

where w^+ and w^- can be treated as the slow varying complex amplitudes of the waves travelling in the positive and negative directions, respectively. If there are no perturbations, the two waves are independent and can be described by

$$\frac{dW^+}{dx} = -j\beta W^+$$
$$\frac{dW^-}{dx} = j\beta W^- \qquad (2.2)$$

where $\beta = \omega / v$ is the propagation constant on the free surface of the substrate, ω is the angular frequency of the surface acoustic wave, and v is the velocity.

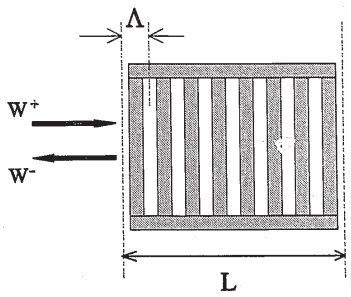

Figure 2.1 SAW Reflection grating

If we use w^+ and w^- as defined above, we get

$$\frac{dw^+(x)}{dx} = -j(\beta - \frac{\pi}{\Lambda})\, w^+(x)$$
$$\frac{dw^-(x)}{dx} = j(\beta - \frac{\pi}{\Lambda})\, w^-(x) \qquad (2.3)$$

When subjected to a perturbation caused by the strips or grooves, the two waves will affect each other. The changes in each of w^+ and w^- are assumed to be a linear function of the amplitude of the wave travelling in the opposite direction. This can be justified when the perturbation is very small because, in this case, the higher order portion can be ignored. In addition, the velocity of the SAW under a short-circuited grating changes, and this results in a change $\Delta\beta$ in the propagation constant. The COM equations for the changes of the complex amplitudes can be written as,

$$\frac{dw^+(x)}{dx} = -j\delta w^+(x) + j\kappa_{12} w^-(x)$$
$$\frac{dw^-(x)}{dx} = j\delta w^-(x) + j\kappa_{21} w^+(x) \qquad (2.4)$$

where

$$\delta = \beta - \frac{\pi}{\Lambda} + \Delta\beta \qquad (2.5)$$

is the detuning parameter and κ_{12} and κ_{21} are the coupling coefficients. By imposing energy conservation, the relation between κ_{12} and κ_{21} is obtained [35],

$$\kappa_{21} = \kappa_{12}^* \equiv \kappa \qquad (2.6)$$

The determinantal equation for the *exp(jλx)* dependence is

$$\lambda = \pm\sqrt{|\kappa|^2 - \delta^2} \tag{2.7}$$

This equation gives the dispersion property of the grating. The dispersion diagram for the single grating is shown in Figure 2.2. We see that, when $|\delta| < |\kappa|$, λ is real and the amplitude of the waves along the grating will either increase or decrease exponentially.

The reflection coefficient for a grating of length L and coupling coefficient κ is,

$$\Gamma(-L) = j\kappa^* \frac{\sinh(\sigma L)}{\sigma\cosh(\sigma L) + j\delta\sinh(\sigma L)} \tag{2.8}$$

where σ is the absolute value of λ.

$$\sigma = \sqrt{|\kappa|^2 - \delta^2} \tag{2.9}$$

At the Bragg frequency, $\delta = 0$ and the magnitude reflection coefficient Γ is a maximum,

$$|\Gamma| = \tanh(\sigma L) \tag{2.10}$$

The dependence of the reflection coefficient of the gratings on frequency and κ is shown in Figure 2.3. We can see that the reflection coefficient approaches unity as σL increases. For $\sigma L = 3$, about 95% of the incident energy is reflected at the Bragg frequency.

The solution of these equations gives the distribution of the wave amplitudes along the gratings for each of the two waves. A matrix notation is more convenient for cascading transmission matrices and will be used in this thesis. If we define

$$w = \begin{bmatrix} w^+ \\ w- \end{bmatrix}, \qquad C = \begin{bmatrix} j\delta & j\kappa \\ -j\kappa^* & -j\delta \end{bmatrix} \tag{2.11}$$

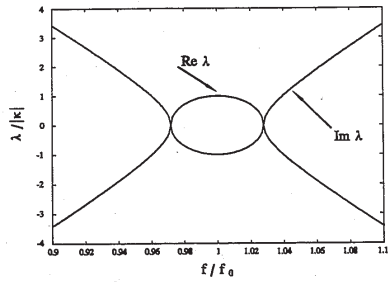

Figure 2.2 The dispersion diagram for SAW grating

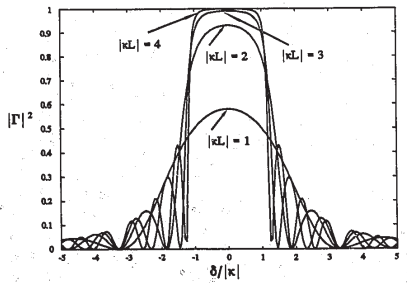

Figure 2.3 The reflection $|\Gamma|^2$ as function of frequency and reflector length

the COM equation (2.4) for gratings can be rewritten as

$$\frac{dw}{dx} = Cw \tag{2.12}$$

The solution for the COM equations is

$$w(x) = V_m E(x) V_m^{-1} w(0) \tag{2.13}$$

where

$$V_m = \begin{bmatrix} V_{11} & V_{12} \\ V_{21} & V_{22} \end{bmatrix}, \qquad E(x) = \begin{bmatrix} e^{\lambda_1 x} & 0 \\ 0 & e^{\lambda_2 x} \end{bmatrix} \tag{2.14}$$

where V_m is eigenvector matrix for matrix C, I_m is the 2×2 unit matrix, and λ_1, λ_2 are the eigenvalues for the matrix C and are given in Eq.(2.7). $w(0)$ is the wave amplitude at a reference position which can be chosen to be any point within the grating.

2.3 COM Theory for Interdigital Transducers

An interdigital transducer (IDT) is shown in Figure 2.4. It is made of a conductive metal film, usually Aluminum. An applied voltage causes stresses between the fingers because of the piezoelectric property of the substrate, and this results in the generation of surface acoustic waves. Since the fingers are periodic, the waves will add in phase at the frequency for which their wavelength is equal to the period of the IDT. In our analysis, we will consider the transducer to be a distributed source of acoustic energy.

In addition to the transduction, the IDT also reflects the surface acoustic waves.

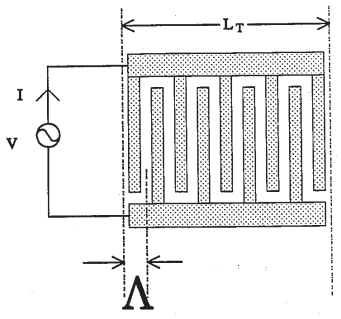

Figure 2.4 SAW interdigital transducer

For a single finger IDT, in particular, the frequency of maximum transduction is the same as the frequency of maximum reflection. The reflection can greatly affect the characteristics of the IDT, and must, therefore, be included in the description for the IDT.

A shorted IDT is essentially the same as a shorted grating, with identical reflections. Further, the transduction of the surface acoustic wave by the electrical voltage is independent of the reflection. The model for reflection gratings can, therefore, be extended to include a transduction term and thus model an IDT. It is assumed that the changes in the complex amplitude of waves are proportional to the applied sinusoidal voltage of angular frequency ω.

A coupling coefficient α is introduced to describe the transduction. For a single-finger IDT, the COM equations can be written as [23]

$$\begin{aligned} \frac{dw^+(x)}{dx} &= -j\delta\, w^+(x) + j\kappa\, w^-(x) + j\alpha V \\ \frac{dw^-(x)}{dx} &= j\delta\, w^+(x) - j\kappa^* w^+(x) - j\alpha^* V \end{aligned} \tag{2.15}$$

The spacial derivative of the current flowing into the IDT fingers can be expressed as,

$$\frac{dI}{dx} = j\zeta\, w^+(x) + j\eta\, w^-(x) + j\omega C_o V \tag{2.16}$$

By applying energy conservation and time reversal arguments, Chen and Haus [23] proved that

$$\zeta = -2j\alpha^* \quad \text{and} \quad \eta = -2j\alpha$$

Hence equation (2.16) becomes,

$$\frac{dI}{dx} = -2j\alpha^* w^+(x) - 2j\alpha\, w^-(x) + j\omega C_o V \tag{2.17}$$

where C_o is the static capacitance per unit length of the IDT.

From the COM equations (2.15) and (2.17), the electro-acoustical characteristics

of the IDT can be described. The transduction coefficient α is related to the midband radiation conductance G_o of the IDT. Following the procedure in [23], the midband radiation conductance of the IDT of N_T finger pairs can be written as

$$G_o = 2|\alpha|^2(2N_T\Lambda)^2 = 8|\alpha|^2 N_T^2\Lambda^2 \tag{2.18}$$

From the equivalent circuit model[41,43], the radiation conductance of IDT at midband can also be expressed as $G_o = 8k^2C_sf_oN_T^2$. Where k^2 is the electromechanical coupling constant, C_s is the static capacitance per electrode pair and f_o is the center frequency of the IDT. Therefore α can be obtained from (2.18) and the radiation conductance expression. The transduction coefficient α is pure real for the single electrode IDT on the substrates discussed in this thesis. The reflection coefficient κ depends on the substrate, the metal film thickness, and can be determined by experimental means. Theoretical analysis can also be applied to obtain the COM parameters [23, 36].

The closed-form solution for the COM equations (2.15) and (2.17) can be obtained when α and κ are independent of x. This is the case of the unapodized IDT, which is widely used in resonator structures.

In matrix form, the COM equation (2.15) for an IDT can be rewritten as

$$\frac{dw}{dx} = Cw + f \tag{2.19}$$

where f is matrix given by

$$f = \begin{bmatrix} j\alpha V \\ -j\alpha^* V \end{bmatrix} \tag{2.20}$$

The solution for equation (2.19) is

$$w(x) = V_m E(x) V_m^{-1}\, w(0) + (V_m E(x) V_m^{-1} - I_m) C^{-1} f \tag{2.21}$$

where

$$V_m = \begin{bmatrix} V_{11} & V_{12} \\ V_{21} & V_{22} \end{bmatrix}, \qquad E(x) = \begin{bmatrix} e^{\lambda_1 x} & 0 \\ 0 & e^{\lambda_2 x} \end{bmatrix} \tag{2.22}$$

Here, $w(0)$ is the wave amplitude at the reference position, which can be chosen to be any point within the IDT.

If the reference is chosen at one end of the IDT and if the IDT length is L, then the relationship between the waves at the two ends and the applied voltage can written as

$$w(L) = V_m E(L) V_m^{-1}\, w(0) + (V_m E(L) V_m^{-1} - I_m) C^{-1} f \tag{2.23}$$

The electrical current in the interdigital transducers can be expressed from the wave solutions at both ends by integrating the current equation (2.18) along x direction.

$$I = NV_m\Lambda_m^{-1}(E(L)-I_m)V_m^{-1}w(0) + N(V_m\Lambda_m^{-1}(E(L)-I_m)V_m^{-1} - I_mL_T)C^{-1}f + j\omega C_T V \tag{2.24}$$

where N is defined as

$$N = \begin{bmatrix} -2j\alpha^* & -2j\alpha \end{bmatrix} \tag{2.25}$$

and Λ_m is defined as,

$$\Lambda_m = \begin{bmatrix} \lambda_1 & 0 \\ 0 & \lambda_2 \end{bmatrix} \tag{2.26}$$

The derivation of the expression is included in the appendix.

2.4 COM Theory for Coupled Waveguides

We have the COM description of the single track gratings and transducers and it can be used in the analysis of the devices composed of IDTs and gratings, such as one-pole resonators and longitudinally coupled resonators. The theory will be used in the analysis of the single track devices in next chapter.

For waveguide coupled resonator, the parallel reflection gratings and transducers are coupled through the evanescent energy distribution. We therefore need a theory to describe the coupling. A coupled grating, shown in Figure 2.5, guides the waves in addition to reflecting them. The approximate fundamental transverse mode profiles are shown in the figure.

The waves on each track are coupled due to the existence of the reflection gratings. This kind of coupling can be described using the same COM theory as that for single gratings. In addition to the reflection, there is also coupling between waves in the same direction on adjacent tracks. This coupling is very similar to the coupling observed in the optical waveguide couplers, where two optical waveguides are coupled through their fringing fields. The theory for optical waveguide couplers is well documented in the literature [35, 38], and we will use it to describe the coupling of acoustic waves travelling in the same direction on parallel track.

In this section, the COM description of the optical waveguide coupler will be reviewed [35]. We will apply the result to the coupled gratings and coupled transducers in the next sections.

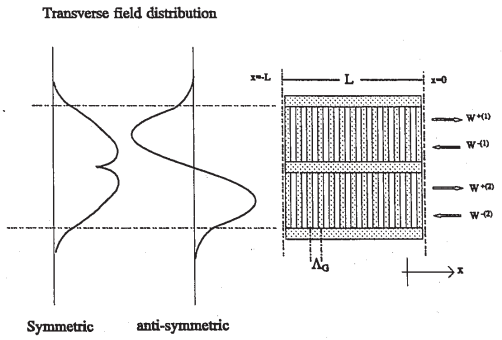

Figure 2.5 SAW coupled reflection grating

Two optical waveguides are shown in Figure 2.6. W_1 and W_2 are two waves, with modes 1 and 2, respectively. In the absent of coupling, they have propagation constants β_1 and β_2 and obey the equations

$$\frac{dW_1}{dx} = -j\beta_1 W_1$$
$$\frac{dW_2}{dx} = -j\beta_2 W_2 \qquad (2.27)$$

Suppose that the two waves are weakly coupled by some means, so that W_1 is affected by W_2, and W_2 is affected by W_1. Then the above equations become

$$\frac{dW_1}{dx} = -j\beta_1 W_1 + j\mu_{12} W_2$$
$$\frac{dW_2}{dx} = -j\beta_2 W_2 + j\mu_{21} W_1 \qquad (2.28)$$

If power conservation is to be observed, then some restrictions must be imposed on κ_{12} and κ_{21}. By applying the energy conservation and time reversal requirement for the lossless passive system, the relation between μ_{12} and μ_{21} becomes [35]

$$\mu_{12} = \mu_{21}^* \equiv \mu \qquad (2.29)$$

If the waves are assumed to have an $\exp(-j\beta x)$ dependence, then the propagation constant for the coupled waves becomes

$$\beta = \frac{\beta_1+\beta_2}{2} \pm \sqrt{\left(\frac{\beta_1-\beta_2}{2}\right)^2 + |\mu|^2} \qquad (2.30)$$

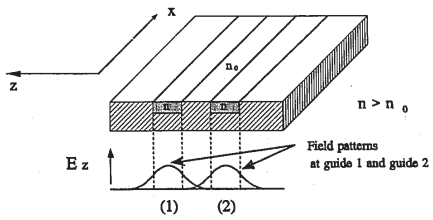

Figure 2.6 Optical waveguide coupler

The solution for the waveguide coupler is

$$W_1(x) = \left[W_1(0)\left(\cos(\beta_o x) + j\frac{\beta_2-\beta_1}{2\beta_o}\sin(\beta_o x)\right) + \frac{j\mu_{12}}{\beta_o} W_2(0)\sin(\beta_o x)\right] e^{-j\frac{\beta_1+\beta_2}{2}x}$$
$$W_2(x) = \left[\frac{j\mu_{21}}{\beta_o} W_1(0)\sin(\beta_o x) + W_2(0)\left(\cos(\beta_o x) + j\frac{\beta_1-\beta_2}{2\beta_o}\sin(\beta_o x)\right)\right] e^{-j\frac{\beta_1+\beta_2}{2}x} \qquad (2.31)$$

where

$$\beta_o = \sqrt{\left(\frac{\beta_1-\beta_2}{2}\right)^2 + |\mu|^2} \qquad (2.32)$$

If the two waveguides are identical ($\beta_1 = \beta_2$), then $\beta_o = |\mu|$ and

$$W_1(x) = [W_1(0)\cos(\beta_o x) + W_2(0)\sin(\beta_o x)]e^{-j\beta_o x}$$
$$W_2(x) = [W_1(0)\sin(\beta_o x) + W_2(0)\cos(\beta_o x)]e^{-j\beta_o x} \qquad (2.33)$$

Consider the situation of an incident wave on one of the waveguides so that $W_1(0) = 1$ and $W_2(0) = 0$. The resulting energy distribution along the travelling direction of the wave is plotted in Figure 2.7. At $x = 0$, the energy of the wave is only in guide one. As it travels along the waveguide, the energy in guide 1 will be transferred to guide 2. After a distance of $|\pi/(2\mu)|$, the energy originally in guide 1 is totally transferred to guide 2. We note that the length required for total transfer from one track to the other is inversely proportional to the coupling coefficient.

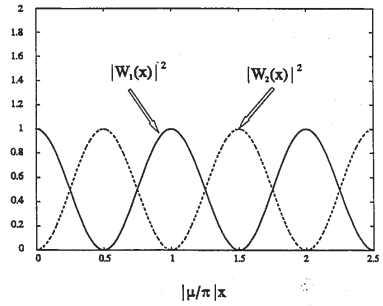

Figure 2.7 The energy distribution along the optical waveguide coupler

2.5 COM Theory for Coupled Gratings

The coupled grating has two tracks as shown in Figure 2.5. Each track can be viewed as a waveguide with periodic perturbation, just as for a conventional reflection grating. The difference is that the waves in the two tracks are now coupled.

The metallization of the grating in the waveguide-coupled resonator serves two purposes. One is the reflection of the surface wave near the Bragg frequency. The other is the guiding effect on the SAW, which is used to control the coupling between the two tracks.

The SAW velocity in the grating region is slower than that of the metallized region and the SAW velocity of metallized region is in turn slower than that of the free surface. Therefore, the wave is guided by the grating metallization and each track can be treated as a waveguide.

The waveguide can support several transversal mode distributions, depending on the velocity difference between the different regions. If the wave reflection is not considered, the two gratings form a coupled acoustic waveguide which is very similar to the optical waveguide coupler. This coupled waveguide will support some guided modes, each of which will have its own phase velocity and transversal profile. The analysis of the transversal modes for such a structure can be borrowed from results obtained in optoelectronics [19, 20].

The COM equations for the coupled grating should account for the reflection of the waves and the waveguide coupling of the waves. The reflection of the waves can be

treated as the coupling of the waves in same track in the opposite direction. While the waveguide coupling between the two tracks can be treated as the coupling of the waves in the same direction between the two track.

We will develop the COM equations for coupled gratings and coupled transducers based on the above assumptions. We can consider wave reflection in the same way as for the single-track gratings and IDTs, by assigning the COM parameter κ to describe it. The coupling between the two gratings and transducers can be considered to be the same as that for the optical waveguide coupler discussed above. The COM equations for the coupled gratings can therefore be obtained by adding the coupling between waves in the same direction in the two tracks to the COM equations (2.4) for single track gratings. A coupling coefficient μ is introduced to describe such coupling. We can then write the COM equations for coupled gratings as

$$\begin{aligned}
\frac{dw^{+(1)}}{dx} &= -j\delta\, w^{+(1)} + j\kappa w^{-(1)} + j\mu\, w^{+(2)} \\
\frac{dw^{-(1)}}{dx} &= -j\kappa^* w^{+(1)} + j\delta\, w^{-(1)} - j\mu^* w^{-(2)} \\
\frac{dw^{+(2)}}{dx} &= j\mu^* w^{+(1)} - j\delta\, w^{+(2)} + j\kappa w^{-(2)} \\
\frac{dw^{-(2)}}{dx} &= -j\mu\, w^{-(1)} - j\kappa^* w^{+(2)} + j\delta\, w^{-(2)}
\end{aligned} \tag{2.34}$$

where the $w^{\pm}$ denote the waves travelling in the positive and negative directions, and the (1) or (2) superscripts denote the track.

The solution of the above equations can be more easily obtained if we write the equations in matrix form, as was done in previous sections. Here

$$\frac{dw}{dx} = C\, w \tag{2.35}$$

where

$$w = \begin{bmatrix} w^{+(1)} \\ w^{-(1)} \\ w^{+(2)} \\ w^{-(2)} \end{bmatrix}, \quad C = \begin{bmatrix} -j\delta & j\kappa & j\mu & 0 \\ -j\kappa^* & j\delta & 0 & -j\mu^* \\ j\mu^* & 0 & -j\delta & j\kappa \\ 0 & -j\mu & -j\kappa^* & j\delta \end{bmatrix} \tag{2.36}$$

The COM parameter μ is assumed to be a real number in the context of this thesis.

The determinantal equation for an assumed $\exp(\lambda x)$ dependence is

$$\lambda = \pm\sqrt{\kappa^2 - (\delta \pm \mu)^2} \tag{2.37}$$

These are also the eigenvalues of the matrix C.

Equation (2.37) is the dispersion relation for the coupled gratings. There are two sets of dispersion curves, as shown in Figure 2.8. The shape of the curves is the same as that for single track gratings. But the curve for each mode has its own Bragg frequency. The two sets of solutions correspond to the symmetric and anti-symmetric modes, respectively, in the transversal direction. This can be verified by examining the eigenvectors corresponding the eigenvalues.

These results agree with the mode description obtained by waveguide analysis [19, 20]. Since the perturbation in x-direction has a fixed periodicity, the two modes must have different Bragg frequencies and different phase velocities. In Eq.(2.37), let $(\delta \pm \mu)=0$, the two solutions for δ corresponse the two Bragg frequencies. The relation between μ

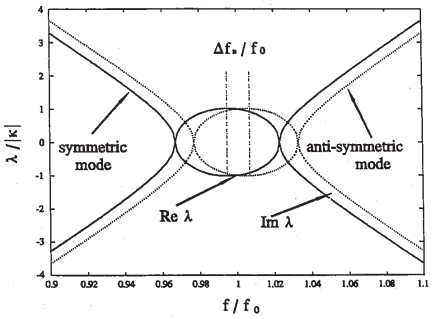

Figure 2.8 The dispersion diagram for SAW coupled grating

and the Bragg frequency difference can be obtained from equations (2.37) and (2.5).

$$\mu = \pi \frac{\Delta f_B}{v} \tag{2.38}$$

where Δf_B is the Bragg frequency difference between the symmetric and anti-symmetric modes. This equation provides a method for calculating the coupling coefficient μ. The difference in Bragg frequencies can be obtained from the theoretical analysis using the waveguide model [19, 20]. Alternatively, μ can be estimated using expressions derived from the optical waveguide couplers [35].

The relation between the two transversal modes can be obtained from the solution of COM equations for a coupled grating. If the COM parameters are known, the response of such a coupled grating can be computed and the relationship between the acoustic waves at the two ends can be expressed in terms of a transmission matrix.

The solution of the coupled grating can be expressed by

$$w(x) = V_m E(x) V_m^{-1} w(0) \tag{2.39}$$

where

$$E(x) = \begin{bmatrix} e^{\lambda_1 x} & 0 & 0 & 0 \\ 0 & e^{\lambda_2 x} & 0 & 0 \\ 0 & 0 & e^{\lambda_3 x} & 0 \\ 0 & 0 & 0 & e^{\lambda_4 x} \end{bmatrix} \tag{2.40}$$

and V_m is the 4 x 4 eigenvector matrix for C and $w(0)$ is the wave amplitude at the reference position.

For a coupled grating having length L, the relationship between the wave

amplitudes at the two ends can be written as

$$w(-L) = V_m E(-L) V_m^{-1} w(0) \tag{2.41}$$

The coupled grating can then be described by the transmission matrix

$$T = V_m E(-L) V_m^{-1} \tag{2.42}$$

2.6 COM Theory for Coupled Interdigital Transducers

Because waveguide-coupled SAW resonators are usually built on ST-X Quartz, the transducers are generally very long and therefore exhibit an extended coupling region. As for the coupled gratings, the waves travelling in the same direction between the two tracks are coupled and the COM theory for a single track IDT should be modified to accommodate the coupling. The structure of the coupled transducer is shown in Figure 2.9. If the input and output of the coupled transducer are shorted, the coupled transducer is a coupled grating. The COM equations for coupled transducers can be obtained by adding the transduction terms to the COM equations for coupled gratings that were previously obtained. Here, it is assumed that the transduction only occurs in the track in which the transducer is located. A transduction term can then be added to the COM equations for coupled gratings, as was done for single-track IDTs. The COM equations

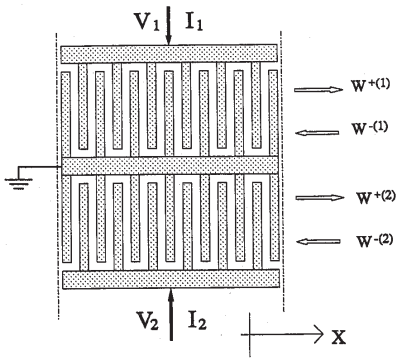

Figure 2.9 SAW coupled transducer

for coupled transducers become

$$\begin{aligned}
\frac{dw^{+(1)}}{dx} &= -j\delta w^{+(1)} + j\kappa w^{-(1)} + j\mu w^{+(2)} + j\alpha V_1 \\
\frac{dw^{-(1)}}{dx} &= -j\kappa^* w^{+(1)} + j\delta w^{-(1)} + j\mu^* w^{-(2)} - j\alpha^* V_1 \\
\frac{dw^{+(2)}}{dx} &= j\mu^* w^{+(1)} - j\delta w^{+(2)} + j\kappa w^{-(2)} + j\alpha V_2 \\
\frac{dw^{-(2)}}{dx} &= -j\mu w^{-(1)} - j\kappa^* w^{+(2)} + j\delta w^{-(2)} - j\alpha^* V_2
\end{aligned} \tag{2.43}$$

The current in each transducer is assumed to be affected by the waves on its own track. We get

$$\begin{aligned}
\frac{dI_1}{dx} &= -2j\alpha^* w^{+(1)} - 2j\alpha w^{-(1)} + j\omega C_o V_1 \\
\frac{dI_2}{dx} &= -2j\alpha^* w^{+(2)} - 2j\alpha w^{-(2)} + j\omega C_o V_2
\end{aligned} \tag{2.44}$$

Thus, the complete COM description of the coupled IDT is obtained. The solution to the equations gives the relation between the waves at each of the two acoustical ports and the electrical port.

The solution for the coupled IDT can be written in matrix form

$$w(x) = V_m E(x) V_m^{-1} w(0) + (V_m E(x) V_m^{-1} - I_m) C^{-1} f \tag{2.45}$$

where V_m and $E(x)$ are the same as those for the coupled gratings, I_m is the 4 × 4 unit matrix. f is given by

The currents in two IDTs are expressed as,

$$f = \begin{bmatrix} j\alpha V_1 \\ -j\alpha^* V_1 \\ j\alpha V_2 \\ -j\alpha^* V_2 \end{bmatrix} \tag{2.46}$$

$$\begin{aligned}
\begin{bmatrix} I_1 \\ I_2 \end{bmatrix} &= N V_m \Lambda_m^{-1} (E(L_T) - I_m) V_m^{-1} w(0) \\
&+ N(V_m \Lambda_m^{-1} (E(L_T) - I_m) V_m^{-1} - I_m L_T) C^{-1} f + j\omega C_T \begin{bmatrix} V_1 \\ V_2 \end{bmatrix}
\end{aligned} \tag{2.47}$$

where N is

$$N = \begin{bmatrix} -2j\alpha^* & -2j\alpha & 0 & 0 \\ 0 & 0 & -2j\alpha^* & -2j\alpha \end{bmatrix} \tag{2.48}$$

and Λ_m is defined as,

$$\Lambda_m = \begin{bmatrix} \lambda_1 & 0 & 0 & 0 \\ 0 & \lambda_2 & 0 & 0 \\ 0 & 0 & \lambda_3 & 0 \\ 0 & 0 & 0 & \lambda_4 \end{bmatrix} \tag{2.49}$$

The derivation of this expression is included in the appendix.

From the solution for the coupled interdigital transducers, we can get the relation between the waves at the both ends for given electrical voltages V_1 and V_2. The electrical currents I_1 and I_2 are also expressed as the function of electrical voltages V_1 and V_2 and the wave amplitudes at one end of the coupled transducers.

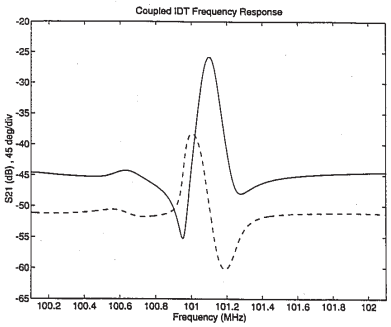

Figure 2.10 Frequency response S_{21} of the coupled transducer (a) Simulation (b) The experimental results

A comparison between theoretical and experimental frequency response of a coupled IDT is given in Figure 2.10. The coupled transducer of 351 fingers was built on ST-Quartz. The aperture of each track is about 8 wavelengths at 100 MHz. The gap between the two tracks is 1.5 wavelengths. The Aluminum film thickness is about 6000Å. We can see that the theoretical result agrees well with the experiment.

2.7 Conclusion

In this chapter, COM theory for single-track SAW gratings and IDTs has been reviewed. COM equations for coupled gratings and coupled transducers have been derived by combining the COM theory used in optical waveguide couplers with the theory for single-track gratings and IDTs. A coupling coefficient μ was introduced to describe the coupling that occurs between the waves propagating in the same direction on adjacent tracks.

In this theory, two different velocities for the symmetric and anti-symmetric modes were observed, with corresponding Bragg frequencies. This result agrees with previously reported mode analysis theories [19,20].

The COM theory for coupled gratings and coupled IDT structures describes the relations between the waves and forms the foundation needed to calculate the frequency response of SAW waveguide-coupled resonators. Another feature of this theory is that the longitudinal mode profile for the waveguide-coupled resonator can be calculated for

a given structure. The longitudinal profile is very important in characterizing the device and in its design. This longitudinal mode profile calculation has not previously been reported in the public literature.

The coupled IDT response calculated from the theory was shown to agree well with experimental results. In next two chapters, the COM theory developed in this chapter will be used to analyze SAW resonators, longitudinally-coupled resonators, and waveguide-coupled resonators.

CHAPTER 3

TWO-PORT RESONATORS AND LONGITUDINALLY COUPLED RESONATORS

3.1 Introduction

Both the longitudinal coupled resonator and the waveguide coupled resonator are acoustically coupled resonators. Two or more acoustic resonant modes can be used in the coupling though, in practice, only two resonant modes are used. The two-pole coupled resonators are the basic building blocks for multi-pole resonators.

Since surface acoustic waves propagate in two dimensions on the surface of the substrate, SAW device can be considered as two-dimensional. Confinement of acoustic energy in these two dimensions is needed in order to produce resonances. The confinement is provided by the reflections in the longitudinal direction and by the guiding effect of gratings in the transverse direction. For single pole resonators, there is only one resonant mode. For two-pole longitudinally coupled resonators, there are two resonant modes having two different longitudinal field distributions with the same transverse field distribution. For two-pole waveguide coupled resonators, there are two resonant modes having two transverse filed distributions with the same longitudinal filed distribution.

The longitudinally-coupled resonator filters are generally built on substrate with a high electro-mechanical coupling coefficient. The coupling between the two modes can be very strong, producing a fractional bandwidth in the order of 1 to 5 percent. Since the

input and output IDTs are on the same track, the out-of-band rejection for this type of resonator filter is lower than that for waveguide-coupled resonators.

Waveguide-coupled resonators are generally built on ST-X quartz which has a lower electro-mechanical coupling coefficient and a very small temperature coefficient, crucial for narrow-band filter applications. The bandwidth of this device is very narrow because of the weak coupling between the two resonators. Since the input and output IDTs are not on the same track, and there is very little coupling between the two tracks outside the stopband of gratings, and this type of resonator filter exhibits excellent out-of-band rejection.

In practical applications, the out-of-band rejection can be further enhanced by electrically cascading two-pole resonators to form multi-pole resonator filters. Since the energy is confined between the reflectors in the resonator structure, filters with very low insertion loss can be obtained when the device is well matched.

The electrical characteristics of the these devices can be analyzed using the COM models for the gratings, IDTs, coupled gratings and coupled transducers. The admittance (Y) matrix can be calculated over the frequency range of interest and used to obtain the scattering (S) matrix.

3.2 The Y and S Parameters

SAW resonators are passive two-port devices. The electrical characteristics of a two-port network can be described using the admittance (or Y) matrix in the frequency

range of interest. Since the electrical variables used in the COM equations are voltage and current, this is a convenient way to characterize the electrical properties. In microwave measurements, however, the characteristics of a two-port device are usually represented by the scattering (or S) matrix. Therefore we need to convert the Y matrix to the S matrix in order to compare with the measurement results. In the following, the definition and the relation between the admittance and the scattering matrices are discussed.

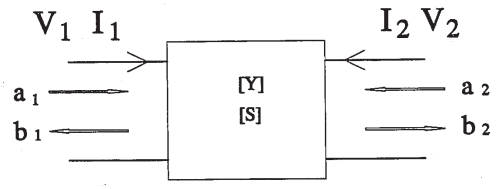

Figure 3.1 Two-port network

Consider the two-port network shown in Figure 3.1. The voltages at the two ports are V_1 and V_2, and the currents are I_1 and I_2. The Y matrix for the two-port network is

defined by

$$\begin{bmatrix} I_1 \\ I_2 \end{bmatrix} = \begin{bmatrix} Y_{11} & Y_{12} \\ Y_{21} & Y_{22} \end{bmatrix} \begin{bmatrix} V_1 \\ V_2 \end{bmatrix} \tag{3.1}$$

Alternatively, the properties of a two-port network can be described by the scattering matrix. The S matrix gives the relation between the incident/reflected waves at the input and output ports. a_1 and a_2 are the incident waves at the two ports and b_1 and b_2 are the reflected waves at the two ports. The S matrix is defined as,

$$\begin{bmatrix} b_1 \\ b_2 \end{bmatrix} = \begin{bmatrix} S_{11} & S_{12} \\ S_{21} & S_{22} \end{bmatrix} \begin{bmatrix} a_1 \\ a_2 \end{bmatrix} \tag{3.2}$$

The relations between the S matrix elements and the Y matrix elements are [40],

$$\begin{aligned} S_{11} &= \frac{(Y_0 - Y_{11})(Y_0 + Y_{11}) + Y_{12}Y_{21}}{\Delta Y} \\ S_{12} &= -\frac{2Y_{12}Y_0}{\Delta Y} \\ S_{21} &= -\frac{2Y_{21}Y_0}{\Delta Y} \\ S_{22} &= \frac{(Y_0 + Y_{11})(Y_0 - Y_{22}) + Y_{12}Y_{21}}{\Delta Y} \end{aligned} \tag{3.3}$$

where

$$\Delta Y = (Y_{11} + Y_0)(Y_{22} + Y_0) - Y_{12}Y_{21} \tag{3.4}$$

and Y_0 is the source and load admittance at the two ports of the device.

3.3 Two-Port Resonators

A two port resonator is constructed by placing two IDTs in the cavity formed by two reflection gratings with sufficient reflection. The structure of a two-port resonator is shown in Figure 3.2. The input IDT is used for the excitation of the acoustic waves and the output IDT is used for the detection.

The cavity formed between two reflection gratings may support several resonant modes. The placement of the gratings and the IDTs is of paramount importance to ensure that only one resonant mode is strongly coupled to the input/output IDTs in the resonator. Incorrect positioning of either IDT or grating can degrade the electromechanical transduction between the input and output IDTs and the acoustic resonance.

Several resonant modes can exist within the stopband of the gratings, each with its own field distribution. In a one-pole resonator, the input/output IDTs are positioned so that only one resonant mode is strongly excited and detected.

The acoustic fields in the cavity between the gratings are standing waves. Each mode has its own standing wave pattern. A standing wave pattern analysis is very useful in understanding the operation of resonators and other devices such as the SPUDT [11, 41]. For simplicity, we assume that the finger reflection of the IDT can be ignored, that the reflection of the grating is at the edge and that the reflection coefficient is independent of frequency.

The reflection coefficient at the physical edge of the shorted reflector on $LiNbO_3$, for example, is negative [41]. Therefore, there must be a standing wave node at the

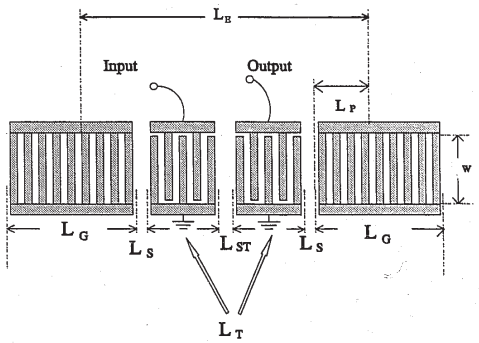

Figure 3.2 Structure of two-port resonator or longitudinally coupled resonator

reflector edges. In addition, the length of the cavity must be an integral number of half wavelengths in order to support the resonant mode. Figure 3.3 shows the standing wave pattern of one possible resonant mode whose resonant frequency is the Bragg frequency of the reflection gratings. An IDT with a synchronous frequency equal to the Bragg frequency of the gratings will have a maximum transduction at this frequency. If the input IDT fingers are at the peaks of the standing wave, maximum coupling will occur. The output IDT will also have maximum coupling to this mode if its fingers are on the standing wave peaks. For such a placement, the IDTs and gratings must be positioned as shown in the Figure 3.3. The distance between the IDTs is an integer number of half wavelength Λ. This is the widely used 'optimal' resonator structure. It has the maximum coupling between the input and output IDTs, and results in the lowest insertion loss and the highest out-of-band rejection.

Another structure that is widely used in the design of SAW resonators is the one with synchronous IDTs. In this structure, each IDT is a periodic extension of the adjacent grating [42, 44]. The standing wave pattern of this structure is shown in Figure 3.4. Unlike the optimal resonator, the IDT fingers are not placed on the peaks of the standing waves and the structure does not provide the maximum coupling between the IDTs and the resonant acoustic mode. The insertion loss is larger than with the optimal design and the out-of-band rejection is lower. Because there is no interruption between the grating and IDT, the effective cavity length is smaller than that of the optimal structure. The advantage of the synchronous resonator is its manufacturability [44] and the relative insensitivity to the reflectivity of the gratings.

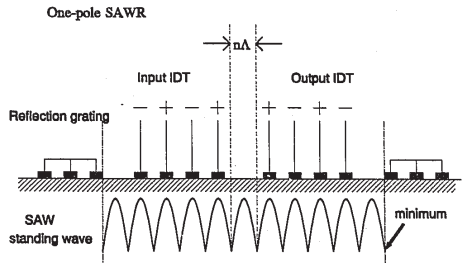

Figure 3.3 Standing wave pattern of two-port resonator with optimal design

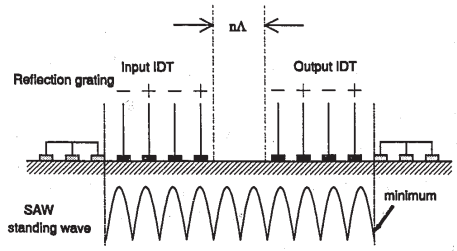

Figure 3.4 Standing wave pattern of two-port resonator with synchronous IDT

From the above discussion, we can see that in one-pole resonators only one mode is coupled to the input and output IDTs. Coupling to the other modes will degrade the performance of the resonator. In the case of coupled resonators, however, the IDTs are designed to have strong coupling to two resonant modes.

3.4 The Longitudinally-Coupled Resonators

The structure of longitudinally-coupled resonators is very similar to the structure of the one-pole two-port SAW resonator in Figure 3.2. This type of device is generally built on highly piezoelectric materials, such as 64° YX $LiNbO_3$ and 36° YX $LiTaO_3$. The lengths of the input and output IDTs are much larger than those for the one-pole resonators. A bandwidth of 1 to 5 percent can be obtained with very low loss and a flat passband between the resonant frequencies of the two modes.

In a longitudinally coupled resonator, two resonant modes are designed to be coupled to the IDTs at both the input and output. The two modes dominate the performance of the device and have a large frequency difference, which makes it possible to produce a wide passband. In this thesis, we will concentrate on the analysis of longitudinally coupled resonators with two IDTs, though it can also be applied to the three-IDT type.

We have seen that in one-pole resonators, the distance between the IDTs is an integer number of half wavelength Λ. In this case, symmetric modes will be coupled to the two IDTs if the distance between the two IDTs is an odd number of periods.

Similarly, only antisymmetric modes are coupled to the two IDTs if the distance is an even number of half wavelength. Within the stopband of the grating and the passband of the IDT, only one of these resonant modes is strongly coupled to the two IDTs.

If the distance between the IDTs is an even number of half wavelengths, the radiation from the two IDTs will cancel near the IDT synchronous frequency when the voltages applied to the two IDTs are in phase. This means that the symmetric mode will not be coupled between the IDTs. On the other hand, if the distance is an odd number of wavelengths, radiation from two IDTs will cancel when the applied voltages are out-off-phase. This means that the anti-symmetric mode is not coupled to the IDTs. Clearly, if two resonant modes are to be equally coupled, the distance between the two IDTs should be an odd number of quarter wavelengths $(2n+1)(\Lambda/2)$.

The standing wave pattern of two resonant modes for a longitudinally coupled resonator is shown in Figure 3.5(a). Here we also assume that the reflection planes are as shown in the figure and that the reflection is independent of frequency. The distance between the IDTs in this device is an integer number and a half grating periods $((n+1/2)\Lambda)$. The distances between IDTs and their adjacent gratings are the same as those for the resonator in Figure 3.2.

Given the length of the cavity, the resonant frequency will be different from the Bragg frequency of the gratings. There are two resonant modes with resonant frequencies around the Bragg frequency. The input and output IDTs are positioned to have almost equal coupling to the two resonant modes. But the phase between the two resonant modes is different, since there is a 180° phase shift between the standing waves on either side

of a node. Figure 3.5(b) shows the longitudinal distribution of the symmetric mode. Figure 3.5(c) shows the anti-symmetric mode standing wave pattern. We will expect a 180° phase difference in the frequency response of the two resonant frequencies. Because there are two resonant modes in the device, it is also called a double mode resonator.

The frequency difference in the two modes can be estimated from the standing wave patterns in Figure 3.5. The cavity length is integer number and a half grating periods due to the postioning of the IDTs and gratings.

$$L_C = \left(m+\frac{1}{2}\right)\Lambda \tag{3.5}$$

where m is an integer. Two resonant modes will exist at frequencies f_1 and f_2, with corresponding wavelengths λ_1 and λ_2. These wavelengths must fulfil the following conditions

$$\begin{aligned}(m+1)\frac{\lambda_1}{2} &= L_C \\ m\frac{\lambda_2}{2} &= L_C\end{aligned} \tag{3.6}$$

These give us the resonant frequencies of the two modes,

$$\begin{aligned}f_1 &= \frac{(m+1)}{m+\frac{1}{2}}f_0 \\ f_2 &= \frac{m}{m+\frac{1}{2}}f_0\end{aligned} \tag{3.7}$$

where f_0 is the Bragg frequency at which the wavelength of the SAW is 2Λ. The

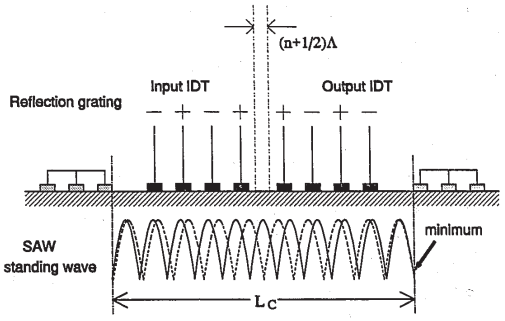

Figure 3.5 (a) The standing wave patterns of the two modes in the longitudinally coupled resonator

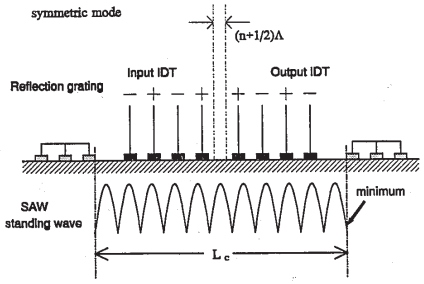

Figure 3.5(b) The symmetric mode standing wave pattern in the longitudinally coupled resonator

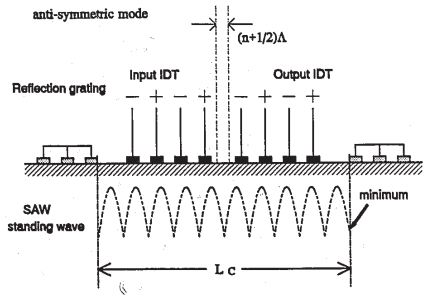

Figure 3.5 (c) The anti-symmetric mode standing wave pattern in the longitudinally coupled resonator

frequency difference of the two modes is

$$\Delta f = f_2 - f_1 = \frac{1}{\left(m+\frac{1}{2}\right)} f_0 = \frac{\Delta}{L_c} f_0 = \frac{v}{2L_c} \tag{3.8}$$

where v is the SAW velocity and L_C is the cavity length.

We can see that the frequency difference between the two modes is inversely proportional to the cavity length. However, in real devices, the standing wave patterns will be more complicated due to the finger reflections from the IDTs. Also, the reflection of the grating is not a perfect mirror as was assumed. The cavity length L_C should be replaced by an equivalent cavity length L_E. The equivalent cavity length of the cavity will be discussed next.

3.5 Equivalent Cavity Length

In the above analysis, we have assumed that the reflection occurs at the physical edges of the gratings and that the reflection is independent of frequency. Actually, because the reflection of the grating is the result of small reflections from the individual reflector strips, the reflection should be considered to occur at some point within the grating. From the COM theory, the reflection coefficient can be expressed in equation (2.8). The phase of the reflection coefficient varies rapidly with frequency, and thus the wave behaves as if it were reflected from a point at some distance into the grating. An

effective cavity length L_E should thus replace L_C in the analysis for longitudinally coupled resonators. This also applies to the analysis of the standard resonators but, in their case, the difference between the resonant frequency and the Bragg frequency is very small. The phase relation between the waves is still valid in the analysis.

The effective reflection point of a grating can be estimated from the frequency response of the gratings. The reflection coefficient of a shorted grating is expressed in equation (2.8). The dependence of the amplitude and the phase of the reflection coefficient on frequency is shown in Figure 3.6(a).

We can estimate the group delay from the phase slope of the reflected waves.

$$\tau = -\frac{d\phi}{d\omega} \tag{3.9}$$

where ϕ is the phase of the reflection coefficient of the reflection grating. The frequency dependence of the time delay is shown in Figure 3.6(b). The corresponding penetration depth is defined as

$$L_P = v(\tau/2) \tag{3.10}$$

We can see that, near the Bragg frequency, the penetration depth is smaller. This is because near the Bragg frequency, the reflection is stronger. For a grating with enough reflection, the penetration depth is almost constant for a very wide band near the Bragg frequency. We can therefore replace the cavity length L_C with a constant equivalent cavity length L_E.

For a given cavity design, a larger reflection from single reflector will lead to a shorter effective cavity length. The reflection coefficient from a single reflector depends

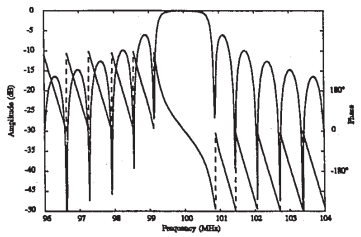

Figure 3.6(a) The amplitude and phase of the reflection coefficient of reflection grating (κ = -900 m^{-1}, 150 metal strips on 128°YX LiNbO3 near 100 MHz)

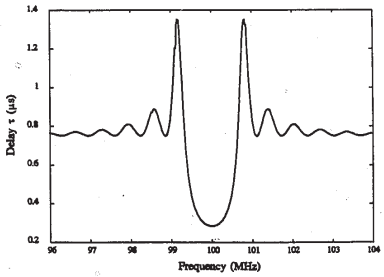

Figure 3.6(b) The delay calculated from the phase of Figure 3.6(a)

on the substrate and on the film thickness. Thicker film will result in a shorter penetration depth, which means a shorter equivalent cavity length and therefore a larger frequency difference between the two modes.

Between the two resonant frequencies, a flat passband can be obtained in the frequency response of a longitudinally coupled resonator with a high electro-mechanical coupling coefficient. This permits the use of the device in wide band filter applications.

A more accurate analysis of the electrical characteristics of resonators and longitudinally coupled resonators needs a computer simulation which can be based on the COM models of the components in the device.

3.6 The Matrix Building Blocks

SAW resonators and longitudinally coupled resonators contain 'building blocks' consisting of gratings, IDTs and acoustic transmission lines. These building blocks can be described by their transmission (ABCD) matrix which gives the relation between the waves at their two ends. The transmission matrix of a structure which contains several building blocks can be easily calculated by cascading the individual transmission matrices.

The transmission matrix of the building blocks are the matrix *G* for SAW reflection gratings, matrix *T* for the IDTs and matrix *D* for acoustic transmission lines. The *G* for gratings and *T* for IDTs can be derived from the COM model for gratings and IDTs in the previous chapter. The transmission line matrix *D* models the delay experienced by the travelling waves [13].

3.6.1 Choice of references and transmission matrix

The relation between the waves at the two ends of a grating can be expressed by the transmission matrix. The COM theory uses a continuous approximation to the discrete periodic reflections from gratings. Although the width of a single reflector is half of the grating period Λ for a grating with a metallization ratio of 0.5, we will assume that it occupies the whole grating period Λ. For the grating array, the end of the grating will be defined at a point a quarter of a grating period from the grating edge, as shown in Figure 3.7(a). Using this definition of the reference planes, the coupling coefficient κ in the COM equation is a real negative number for shorted aluminum gratings on $LiNbO_3$. The reference plane for the IDT is also defined in the same way as for the gratings. This is shown in Figure 3.7(b).

In matrix form, amplitudes of forward and reverse surface acoustic waves at the i^{th} reference axis are

$$W_i = \begin{bmatrix} W_i^+ \\ W_i^- \end{bmatrix} \tag{3.11}$$

The transmission matrix for a grating or delay section is defined as

$$W_{i-1} = G_i W_i \tag{3.12}$$

The 2 × 2 matrix G_i gives the relation of the waves at the two ends. The transmission matrix of a device containing several sections of gratings and transmission lines can be expressed as the multiplication of their transmission matrices.

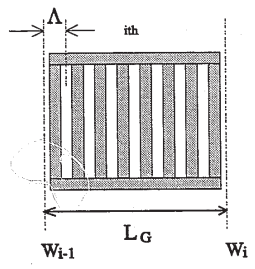

Figure 3.7 (a) The references for the reflection grating

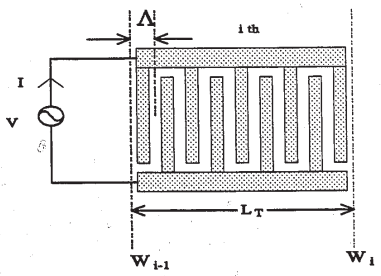

Figure 3.7 (b) The references for the interdigital transducer

3.6.2 Transmission matrix for gratings

The solution for the COM equation in equation (2.13) already gives the relation of the slow varying amplitudes w^+ and w^- at the two ends of the gratings. The amplitudes of the waves at can be obtained from equation (2.1).

As shown in Figure 3.7(a), for a grating containing N_G strips, the length L_G is $N_G\Lambda$. If the right end is chosen as $x = 0$, the wave amplitude relations can be expressed as,

$$\begin{bmatrix} W_{i-1}^{+} \\ W_{i-1}^{-} \end{bmatrix} = (-1)^{N_G} \begin{bmatrix} w_{i-1}^{+} \\ w_{i-1}^{-} \end{bmatrix} \tag{3.13}$$

and

$$\begin{bmatrix} W_i^{+} \\ W_i^{-} \end{bmatrix} = \begin{bmatrix} w_i^{+} \\ w_i^{-} \end{bmatrix} \tag{3.14}$$

The relation between the wave amplitudes at the two ends is

$$W_{i-1} = (-1)^{N_G} V_m E(-L_G) V_m^{-1} W_i \tag{3.15}$$

The transmission matrix for a grating is therefore

$$G_i = (-1)^{N_G} V_m E(-L_G) V_m^{-1} \tag{3.16}$$

3.6.3 Transmission Matrix for IDTs

The IDT shown in Figure 3.7(b) has two acoustic ports and one electrical port. In addition to the transmission matrix which is same as that for gratings, there is another term due to the electrical transduction. The wave amplitude relation can be obtained from the solutions of the COM equations for IDTs. From equation (2.21), the transmission relation between the two ends of the IDT can be written as

$$\begin{aligned} W_i &= (-1)^{N_T} \left(V_m E(L_T) V_m^{-1} W_{i-1} + (V_m E(L_T) V_m^{-1} - I_m) C^{-1} f \right) \\ &= T_i^{-1} W_{i-1} + t_i \end{aligned} \tag{3.17}$$

where N_T is the number of fingers in the IDT, $L_T = N_T\Lambda_T$ is the length of the IDT. T_i is the transmission matrix when the IDT is shorted.

$$T_i = (-1)^{N_T} V_m E(-L_T) V_m^{-1} \tag{3.18}$$

t_i is a 4 × 1 matrix corresponding to the transduction due to the applied voltage.

$$t_i = (-1)^{N_T} \left(V_m E(L_T) V_m^{-1} - I_m \right) C^{-1} f \tag{3.19}$$

The current in the IDT can be obtained from equation (2.24)

$$I_i = N V_m \Lambda^{-1} (E(L_T) - I_m) V_m^{-1} w_{i-1}) + N (V_m \Lambda^{-1} (E(L_T) - I_m) V_m^{-1} - I_m L_T) C^{-1} f + j\omega C_T V \tag{3.20}$$

3.6.4 The transmission matrix for acoustic transmission line

In addition to gratings and IDTs, there are spaces acting as acoustic transmission lines between the gratings and IDTs in resonators and longitudinally coupled resonators.

As shown in Figure 3.7(c), the transmission matrix for a transmission line of length L_D can be expressed as [13],

$$W_{i-1} = D_i W_i \tag{3.21}$$

where

$$D_i = \begin{bmatrix} e^{j\beta L_D} & 0 \\ 0 & e^{-j\beta L_D} \end{bmatrix} \tag{3.22}$$

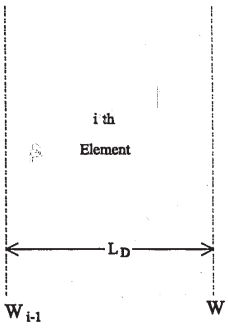

Figure 3.7 (c) The references for the acoustic transmission line

3.7 The Procedure for Simulation

By applying the boundary conditions at the intersections of the elements, the admittance (Y) matrix over the frequency range of interest can be calculated for two-port resonators and longitudinally coupled resonators. Since these two types of resonators have a very similar structure, they can share the computation algorithm for the simulation.

The structure of these two devices is illustrated in Figure 3.8. The input and output IDTs, T3 and T5, are separated by a space D4. Two gratings, G1 and G7, are separated by the two IDTs and the corresponding spaces, D2 and D6.

To determine the value of the waves in the elements of the device, appropriate boundary conditions are necessary. For these, we will assume that there are no incident waves at the far end of the gratings. This condition can be justified by the facts that the reflectors confine the acoustic energy within the cavity and that acoustic absorbers are often placed on the substrate edges. The boundary conditions between the sections are that the waves are continuous. This means that the transmission matrix of two adjacent elements can be written as the multiplication of the transmission matrices of these two elements.

By definition of the Y matrix, the elements of Y_{11} and Y_{21} matrix can be obtained by measuring the currents I_1 and I_2 at the condition of $V_2 = 0$. Then,

$$\begin{aligned} Y_{11} &= \frac{I_1}{V_1}\Big|_{V_2 = 0} \\ Y_{21} &= \frac{I_2}{V_1}\Big|_{V_2 = 0} \end{aligned} \tag{3.23}$$

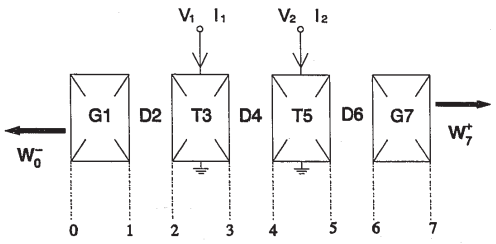

Figure 3.8 The building block illustration for two-port resonator or longitudinally coupled resonator

As shown in Figure 3.8, the section boundaries are marked by numbers. In calculating the Y matrix, we first set the voltage V_2 at the second IDT to zero. The second IDT then behaves as a grating. The wave amplitudes at the two ends of the first IDT (W_2, W_3) can be related to the wave amplitudes at the two ends of the device (W_0, W_7).

$$W_3 = (D_4 T_5 D_6 G_7) W_7 \tag{3.24}$$

and

$$W_0 = (G_1 D_2) W_2 \tag{3.25}$$

The relation between the wave amplitudes of W_2 and W_3 can be expressed by equation (3.17),

$$\begin{aligned} W_3 &= (-1)^{N_T} \left(V_m E(L_T) V_m^{-1} W_2 + (V_m E(L_T) V_m^{-1} - I_m) C^{-1} f \right) \\ &= T_3^{-1} W_2 + t_3 \end{aligned} \tag{3.26}$$

At position 1 and 7, there are no incident waves. Therefore,

$$W_0^+ = 0 \tag{3.27}$$

and

$$W_7^- = 0 \tag{3.28}$$

W_2 is an vector of two elements. From equations (3.24), (3.26) and (3.28), a equation for W_2 is obtained. From equations (3.25) and (3.27), another equation for W_2 is obtained. Therefore, two linear algebra equations with the two unknown variables in W_2 can be obtained. Then W_2 can be solved from the two equations. The current I_1 is calculated from equations (3.14) and (3.20) in terms of V_1.

The second step is to calculate I_2. From the solved W_2, W_3 can be obtained from equation (3.26). W_4 can be obtained from the transmission matrix relation between W_4 and W_3. In the same way as for I_1, I_2 can be calculated from equations (3.14) and (3.20). Then Y_{11} and Y_{21} are obtained from equation (3.23).

Usually, the device is symmetric about the centre of the device. Then we have

$$\begin{aligned} Y_{12} &= Y_{21} \\ Y_{22} &= Y_{11} \end{aligned} \tag{3.29}$$

If the device is not symmetric, Y_{12} and Y_{22} can be calculated in the same way as that for Y_{11} and Y_{21} by setting $V_1 = 0$ as described above.

3.8 Simulation and Experimental Results

The frequency responses of the two-port resonator and longitudinally coupled resonator can be computed from the COM theory by using the procedure described above. In this section, simulation results will be compared with experimental results for devices with various designs. Two one-pole resonators and one longitudinally coupled resonator were designed, simulated, fabricated and measured. The devices were fabricated using the standard lithographic process using chemical etching technique. The devices were measured on network analyzers of 50 Ω system.

3.8.1 The SAW Two-port Resonators

Two SAW two-port resonators were designed and fabricated. One was an optimal resonator, in which the IDT fingers were on the peaks of the standing waves between the two gratings, as analyzed in Figure 3.3. The other was a synchronous design in which the IDT was an extension of the grating. The design parameters of these two devices are listed in Table 3.1

Table 3.1 Design of the two-port resonators

	Device 1 (optimal)	Device 2 (synchronous)
Substrate	YZ $LiNbO_3$	128° YX $LiNbO_3$
Electrodes	Aluminum	Aluminum
Film thickness	5500 Å	5500 Å
IDT period	19.38 μm	19.38 μm
Grating period	19.38 μm	19.38 μm
Number of fingers in one IDT	9	9
Reflectors (per side)	150	150
Aperture (W/(2Λ))	30	30
Spaces between IDT and adjacent grating (Λ)	5.0	5.0
Space between IDTs (Λ)	.75	1.0

(a) Device 1 -- The optimal design

Figure 3.9 shows the radiation conductance at the frequency range near resonance. From the radiation conductance pattern, we can see that there is a sharp peak at the resonant frequency. Since the energy transformed from electrical to acoustic is

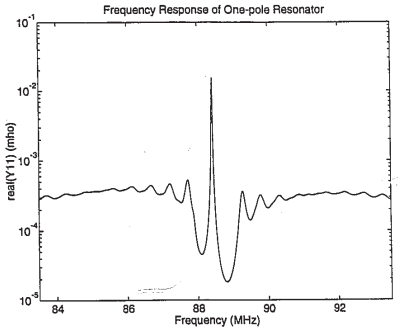

Figure 3.9 The simulation result on the Y_{11} of Resonator 1

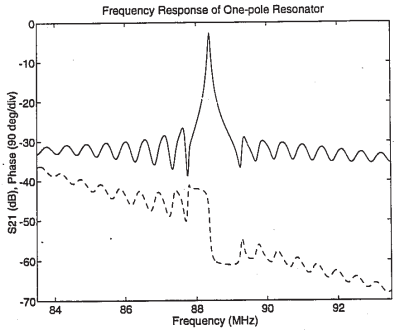

Figure 3.10 (a) The simulation result on the S_{21} of Resonator 1

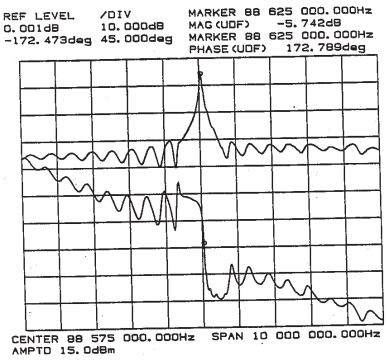

Figure 3.10 (b) The experimental result on the S_{21} of Resonator 1

proportional to the radiation conductance, the energy conversion to acoustic energy is much larger near resonance. There is only one large peak, so the other longitudinal modes are not efficiently excited in this device.

From the admittance matrix, the scattering matrix of the device can be calculated and compared to measurements taken with a network analyzer. The simulated and measured parameters S_{21} are shown in Figure 3.10. We can see that there is very good agreement between the results.

(b) Device 2 -- The synchronous design

The second device had a design which was slightly different from the first. In this device, the distance between the IDTs and their adjacent gratings was changed from 0.75 Λ to 1.0 Λ. This device was not strictly a synchronous design. However, the frequency response of the device should be the same because the reflection coefficient from the grating does not change if the grating is moved by a half wavelength. The frequency response of the radiation conductance, shown in Figure 3.11, has one resonant peak. However, there are now some peaks on the left side of the main peak which are about 15 dB bellow the main peak.

The simulated and measured results for the S_{21} parameter are shown in Figure 3.12. We can see that it exhibits smaller out-of-band rejection when compared to Device 1. The simulation result agrees well once again with the experimental measurement. The small ripples noticeable in the latter can be attributed to the presence of transverse modes.

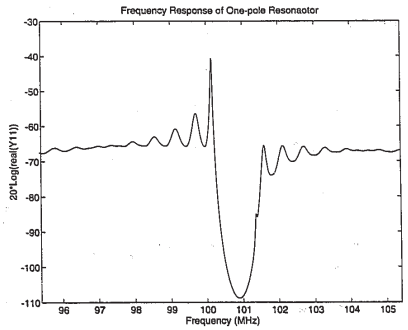

Figure 3.11 The simulation result on the Y_{11} of Resonator 2

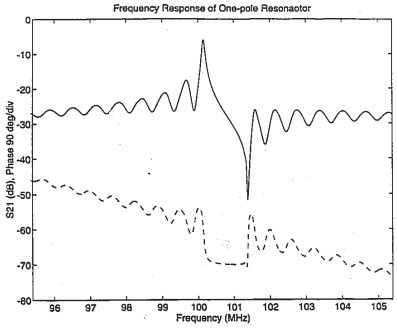

Figure 3.10(a) The simulation result on the S_{21} of Resonator 2

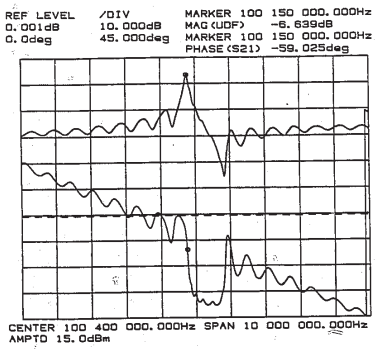

Figure 3.10(a) The experimental result on the S_{21} of Resonator 2

3.8.2 The Longitudinally Coupled Resonator

A longitudinally coupled resonator was designed and fabricated on 128° YX $LiNbO_3$. The electro-mechanical coupling coefficient k^2 of 128° YX $LiNbO_3$ is similar to that of 36° YX $LiTaO_3$. The design parameters for the device are listed in Table 3.2.

Table 3.2 Design of the longitudinally coupled resonator

Substrate	128° YX $LiNbO_3$
Electrodes	Aluminum
Film thickness	6000 Å
IDT period	19.38 μm
Grating period	19.38 μm
Number of fingers in one IDT	51
Reflectors (per side)	150
Aperture (W/(2Λ))	50
Spaces between IDT and adjacent grating (Λ)	.75
Space between IDTs (Λ)	1.5

The distance between the IDTs is such that the symmetric and anti-symmetric modes are excited equally if no reflection occurs in the IDT fingers. The radiation conductance of the longitudinally coupled resonator is shown in Figure 3.13(a). From the figure, we can see that two peaks corresponding to the two longitudinal modes dominate the response. The real part of the Y_{12} is shown in Figure 3.13(b). We can see that the two modes have opposite signs at the output IDT, as expected.

The other difference is that the length of the IDTs is significant longer than that for single-pole resonators. If the IDTs are not long enough, there will be a hump between the two resonance frequencies of the two modes in the S_{21} of the device. Therefore, in

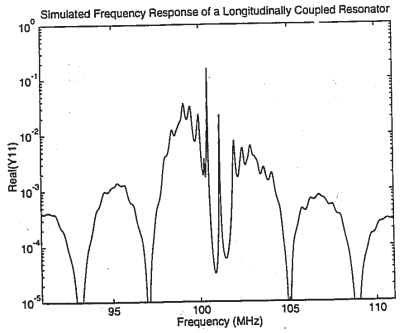

Figure 3.13 (a) The simulation result on the Y_{11} of the longitudinally coupled resonator

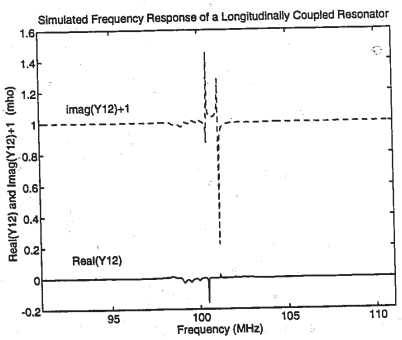

Figure 3.13 (b) The simulation result on the Y_{11} of the longitudinally coupled resonator

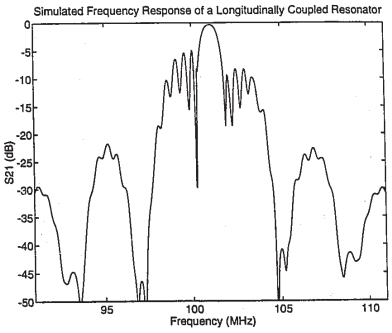

Figure 3.14 (a) The simulation result on the S_{21} of the longitudinally coupled resonator

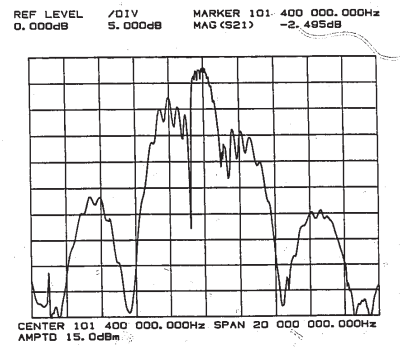

Figure 3.14(b) The Experimental result on the S_{21} of the longitudinally coupled resonator

order to use the coupled resonator, the IDTs must be much longer than for the single-pole resonators.

The simulation and experimental results for S_{21} is shown in Figure 3.14(a) and Figure 3.14(b), respectively. We can see that the results agree well. There are some ripples in the passband of the S_{21} in the experimental result. This is caused by higher order transverse modes. In [39], these ripples were not as prominent, probably because those devices were fabrication on 64° YX $LiNbO_3$ or 36° YX $LiTaO_3$. The acoustic waves on these substrate are leaky surface acoustic waves (LSAW). Higher order transverse modes may not be guided by the metallization on the surface.

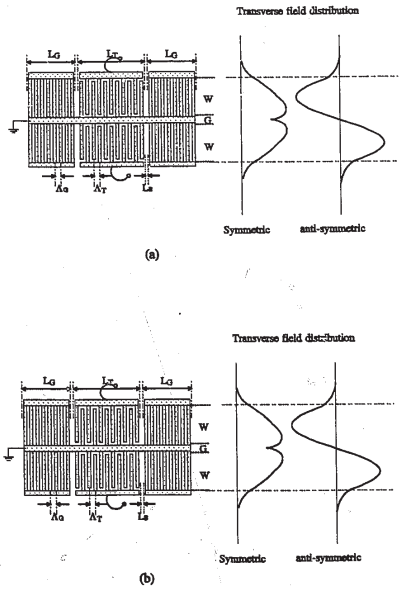

Figure 4.1 Waveguide coupled resonator (a) The finger-out-of-phase structure (b) The finger-in-phase structure

CHAPTER 4

SAW WAVEGUIDE COUPLED RESONATORS

4.1 Introduction

The structure of a double-mode waveguide coupled resonator is shown in Figure 4.1. The device consists of coupled gratings that confine the acoustic energy and lead to resonances, and of coupled transducers that permit the excitation and detection of the acoustic waves. Generally, this type of coupled resonator has a narrow passband of not more than 0.1 percent of the centre frequency and is built on low temperature coefficient materials such as ST-Quartz.

Transversely, the device can be viewed as having two tracks divided by the centre busbar. The velocity of the SAW in the grating region is slower than under the metal busbar and the velocity of SAW under the metal busbar is lower than that of the free surface of the substrate. These velocity differences are dependent on the thickness of the metal film and on the acoustic wavelength, and they produce a guiding effect on the acoustic waves.

The guided modes in each waveguide have an evanescent energy distribution outside the waveguide. Because of the closeness of the two tracks, this evanescent energy distribution produces some energy transfer between the two tracks. For the double-mode waveguide coupled resonator, this coupling will lead to transverse modes across the whole

structure. Of these, the fundamental symmetric and anti-symmetric modes are dominant. The transverse distributions of these two modes are illustrated in Figure 4.1. These two modes are the eigen modes of the coupled waveguide. Standard waveguide analysis predicts that the anti-symmetric mode will have a higher phase velocity than the symmetric mode [19].

In addition to the transverse guiding effects on the SAW, the grating has the important role of confining the waves in the longitudinal direction. In contrast to standard resonators, two resonant modes, corresponding to the two transverse field distributions, are supported. The two modes have the same field distribution in the longitudinal direction, but are different in the transverse direction. Because the two transverse modes have different phase velocities, they will have different Bragg frequencies. This will result in two resonant frequencies. Because one transverse mode is symmetric and the other is anti-symmetric, there is a 180° phase difference between the S_{21} parameter of the two resonant frequencies. This twin peak characteristic will be repeated for each of the longitudinal resonances that can be supported by the resonant cavity.

The electrical characteristics of the waveguide coupled resonator can be analyzed using the COM model developed for the coupled gratings and coupled transducers. The admittance matrix can be computed over the frequency range of interest by applying the appropriate boundary conditions to the transmission relations of the individual components of the device. The design of the device can be optimized based on the simulation results for different device structures.

In this chapter, the COM model for coupled gratings and coupled transducers is

used in the analysis of waveguide coupled resonators. The procedure for the design of the waveguide coupled resonators is discussed. Experimental results are compared with computer simulations based on the COM model. New structures for waveguide coupled resonators with four poles are analyzed. The longitudinal field distributions of the waveguide coupled resonator at resonance are analyzed. Finally, the COM parameters used in the simulation are discussed.

4.2 The Matrix Building Blocks

The electrical characteristics of the waveguide coupled resonators can be analyzed using the matrix building block method which was introduced for the analysis of resonators and longitudinally coupled resonators in Chapter 3. In the same way, the admittance matrix and the scattering matrix of the device can be computed over the frequency range of interest by applying the boundary conditions, between sections and at the ends of the device, to the transmission matrices. For waveguide coupled resonators, the building blocks are coupled gratings, coupled transducers and two-track acoustic transmission lines. The transmission matrix is defined in the same way as that for the single-track gratings and IDTs. But in the case of waveguide coupled resonators, there are waves travelling on two tracks in both directions, giving us 1 × 4 wave amplitude vectors and 4 × 4 transmission matrices. These transmission matrices can be obtained from the COM model for the coupled gratings and transducers. The transmission matrices for coupled gratings and coupled IDTs will be given in the following sections.

4.2.1 The transmission matrix for coupled gratings.

The reference lines for coupled gratings are shown in Figure 4.2. W_{i-1} and W_i are the wave amplitudes at the two ends of the i^{th} section. W_i is defined as,

$$W_i = \begin{bmatrix} W_i^{+(1)} \\ W_i^{-(1)} \\ W_i^{+(2)} \\ W_i^{-(2)} \end{bmatrix}$$

where the + and – symbols denote the travelling direction of the waves and the bracketed (1) or (2) superscripts denote the track.

The transmission relation for the coupled grating is defined as,

$$W_{i-1} = G_i W_i$$

where G_i is the transmission matrix for the coupled grating. It is a 4 × 4 matrix describing the relation between the wave amplitudes at the two ends of the coupled grating.

The transmission matrix of a coupled grating of length $N_G\Lambda$ can be derived from the solution of the COM equations for coupled gratings, as given by equations (2.39) and (2.1). The transmission relation can be expressed as,

$$W_{i-1} = (-1)^{N_G} V_m E(-L_G) V_m^{-1} W_i$$

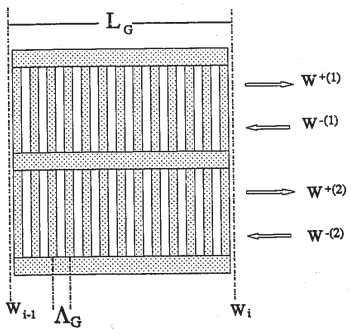

Figure 4.2 References for coupled grating

The transmission matrix for the coupled grating is thus

$$G_i = (-1)^{N_G} V_m E(-L_G) V_m^{-1}$$

The $E(-L_G)$ and V_m are 4 × 4 matrices which were defined in section 2.5.

4.2.2 The transmission matrix for coupled transducers

The coupled transducer has four acoustic ports and two electrical ports. The electrical ports are represented by the voltages V_1 and V_2 and by the currents I_1 and I_2 for the two transducers. The reference lines for the coupled transducer are shown in Figure 4.3. The relation of the wave amplitudes at the two ends of the coupled transducer can derived from the COM solution for coupled transducers. From equations (2.45) and (2.1), the transmission relation for a coupled transducer with N_T fingers can be expressed as,

$$\begin{aligned} W_i &= (-1)^{N_T} \left(V_m E(L_T) V_m^{-1} W_{i-1} + (V_m E(L_T) V_m^{-1} - I_m) C^{-1} f \right) \\ &= T_i^{-1} W_{i-1} + t_i \end{aligned} \qquad (4.5)$$

where $L_T = N_T\Lambda_T$ is the length of the coupled transducer. T_i is the transmission matrix of the coupled transducers when both electrical ports are shorted.

$$T_i = (-1)^{N_T} V_m E(-L_T) V_m^{-1} \qquad (4.6)$$

t_i is 4 × 1 matrix corresponding to the transduction of the applied voltages V_1 and V_2.

$$t_i = (-1)^{N_T} \left(V_m E(L_T) V_m^{-1} - I_m \right) C^{-1} f \qquad (4.7)$$

The currents I_1 and I_2 of the coupled transducer can be obtained from equation (2.47).

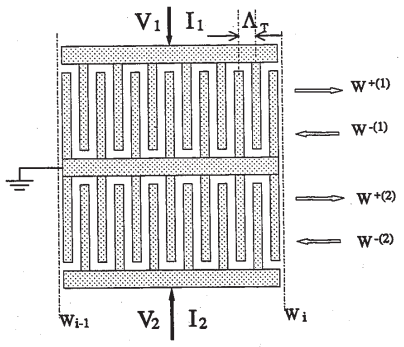

Figure 4.3 References for coupled transducer

The definitions of the matrices and vectors are the same as those given in section 2.6.

$$\begin{bmatrix} I_1 \\ I_2 \end{bmatrix} = NV_m\Lambda_m^{-1}(Z(L_T)-I_m)V_m^{-1}w_{i-1}) + N(V_m\Lambda_m^{-1}(E(L_T)-I_m)V_m^{-1} - I_mL_T)C^{-1}f + j\omega C_T\begin{bmatrix} V_1 \\ V_2 \end{bmatrix} \quad (4.8)$$

4.2.3 The transmission matrix for two-track acoustic transmission lines

The acoustic transmission lines in the waveguide coupled resonators contain two tracks. From equation (3.22), the transmission matrix D_i for the acoustic transmission line of length L_D, shown in Figure 4.4, can be obtained.

$$D_i = \begin{bmatrix} e^{j\beta L_D} & 0 & 0 & 0 \\ 0 & e^{-j\beta L_D} & 0 & 0 \\ 0 & 0 & e^{j\beta L_D} & 0 \\ 0 & 0 & 0 & e^{-j\beta L_D} \end{bmatrix} \quad (4.9)$$

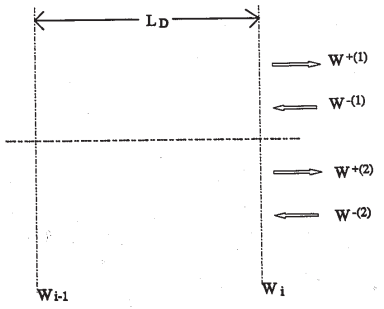

Figure 4.4 References for the two-track acoustic transmission line

4.3 The Procedure for Simulation

The waveguide coupled resonators are two-port devices and can be characterized with the use of the admittance matrix and scattering matrix, as done in the previous chapter for resonators and longitudinally couple resonators. The transmission matrix and the 'building block' concepts can still be applied in the analysis of the WGC resonators.

A waveguide coupled resonator can be described by the five building blocks shown in Figure 4.5. They consist of two coupled reflector gratings (G1 and G5), one coupled transducer (T3) and the spaces (D2 and D4) between the coupled transducer and the two reflector gratings. We will assume that the same boundary conditions of continuous waves and of no incidents waves at the two ends of the device apply.

The transmission matrix between the points 0 and 2 is formed by cascading the two transmission matrices of G1 and D2. Therefore, the transmission relation between the wave amplitude at the two points is

$$W_0 = (G_1D_2)W_2 \quad (4.10)$$

Similarly, the transmission relation between waves at points 3 and 5 is

$$W_3 = (D_4G_5)W_5 \quad (4.11)$$

From equation (4.5), the transmission relation between the two ends of the coupled transducer can be written as

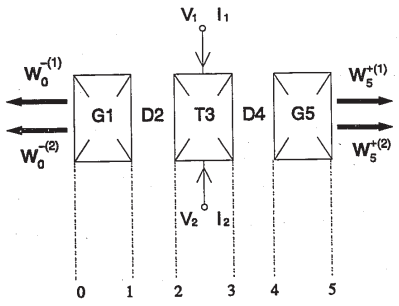

Figure 4.5 The building block illustration for WGC resonator

$$W_3 = (-1)^{N_T}\left(V_m E(L_T) V_m^{-1} W_2 + (V_m E(L_T) V_m^{-1} - I_m) C^{-1} f\right) \quad (4.12)$$
$$= T_3^{-1} W_2 + t_3$$

where f is a vector associated with the applied voltages at the two electrical ports of the coupled transducer. From equation (2.46), it can be expressed as

$$f = \begin{bmatrix} j\alpha V_1 \\ -j\alpha^* V_1 \\ j\alpha V_2 \\ -j\alpha^* V_2 \end{bmatrix} \quad (4.13)$$

Because there are no incident waves at the two ends of the device, the boundary conditions at the two ends of the device (points 0 and 5) can be expressed as,

$$W_0^{+(1)} = 0 \qquad W_0^{+(2)} = 0 \quad (4.14)$$

and

$$W_5^{-(1)} = 0 \qquad W_5^{-(2)} = 0 \quad (4.15)$$

Equations (4.10) and (4.14) give us two equations for W_2. Another two equations for W_2 can be obtained from equations (4.11), (4.12) and (4.15). Therefore, we have four equations for the four unknown values in the 1×4 wave amplitude vector W_2.

The currents I_1 and I_2 can be obtained from the solution of W_2 and the applied voltages by using equation (4.8).

$$\begin{bmatrix} I_1 \\ I_2 \end{bmatrix} = N V_m \Lambda_m^{-1}(E(L_T)-I_m) V_m^{-1} w_2 + N(V_m \Lambda_m^{-1}(E(L_T)-I_m) V_m^{-1} - I_m L_T) C^{-1} f \quad (4.16)$$
$$+ j\omega C_T \begin{bmatrix} V_1 \\ V_2 \end{bmatrix}$$

where w_2 is the slow varying wave amplitude vector. From equation (2.1),

$$w_2 = (-1)^{N_T} W_2 \quad (4.17)$$

From the definition of the Y matrix, the Y_{11} and Y_{21} elements can be computed by setting $V_2 = 0$. Then Y_{11} and Y_{21} can be expressed as the ratio of the currents I_1 and I_2, respectively, to the applied voltage V_1. Y_{22} and Y_{12} can be computed in the same way as Y_{11} and Y_{21}. Usually, the device is symmetric about the centre busbar. Then

$$Y_{22} = Y_{11} \qquad Y_{12} = Y_{21} \quad (4.18)$$

The scattering matrix (S) parameters can be computed from the admittance matrix by using equations (3.3) and (3.4) in section 3.2.

4.4 The Design Procedure for WGC Resonators

The substrate, the metal film, and the film thickness are the material parameters in the design of WGC resonators. The other aspect is the device geometry. This includes the periodicity of the gratings and of the transducers, the aperture of the device, the lengths of the coupled gratings and transducers and the spaces between the coupled transducers and the gratings. Here, general guidelines in choosing these parameters are given.

Because the bandwidth of the WGC resonator is small (< 0.1%), good temperature stability of the substrate is crucial in practical application. Almost all WGC resonators are fabricated on ST-Quartz.

The Aluminum coupled reflector gratings and coupled transducers are deposited on the surface of the substrate using a standard lithographic process. For the purpose of this thesis, the fabrication was done using chemical etching. Since the electro-mechanical coupling coefficient of the ST-quartz is very small, the grating reflection and guiding effect are dominated by mass loading. This requires a film of sufficient thickness.

The most important specifications for the electrical performance of a WGC resonator are the centre frequency and bandwidth. The centre frequency of the device is determined by the period of the coupled gratings and by the period of the coupled transducer. Normally, the coupled transducer is designed to have a similar periodicity as that of the reflection gratings. In most cases, they have the same finger/electrode widths and the metallization ratio of 0.5, producing a finger/electrode width of a quarter wavelength of the SAW at the centre frequency of the device.

The bandwidth of the WGC resonator depends on the frequency difference between the two transverse modes, and therefore on the coupling between the two resonators. The frequency difference between the two resonance modes is determined by the aperture, by the gap between the two tracks and by the film thickness of the device.

The relative frequency difference between the two resonant modes was studied analytically and experimentally by Tanaka *et al* [19]. The results are shown in Figure 4.6. We can see that there is a discrepancy between the experimental and analytical results.

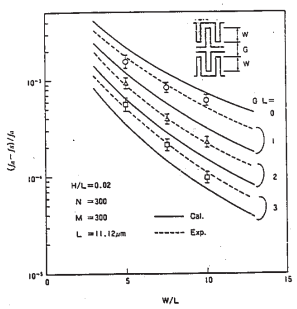

Figure 4.6 The dependence of the frequency difference of the two transverse modes (from [19], reprinted with permission from IEEE, ©1984 IEEE) (L = 2Λ, Λ is the grating period. H is the film thickness, H/L = 0.02)

but that the trend of the dependence on W and G is correct. This discrepancy was later explained by Hunt *et al* [20] by taking into account the anisotropy of ST-Quartz. In Figure 4.6, we see that the relative frequency difference and the acoustical coupling between the two modes is more strongly affected by the gap of the common busbar than by the aperture W of each track. In practice, the aperture of each track is chosen to be between 5 and 20 λ. The gap G is usually below 3 λ [45].

In addition to the aperture W and the gap G between the two tracks, the other parameters required in defining a WGC resonator are the length of the reflector gratings, the length of coupled transducer, and the spaces between elements. The reflector grating should be long enough to produce substantial reflection. Generally, 200 to 300 reflector strips are needed in the device. The length of the coupled transducer is determined by the impedance requirement.

Because the electro-mechanical coupling coefficient of ST-Quartz is very small and the aperture of the transducer is restricted for substantial acoustic coupling between the two tracks, a large number of fingers is needed in the coupled transducer to produce adequate electro-acoustic transduction. This number affects the impedance character of the device. Generally, the number of fingers is between 300 to 600.

Because of the large transducer length, which results in a long cavity length, several longitudinal modes are possible within the passband of the coupled transducer. Therefore, spurious longitudinal modes may exist in the frequency response. These longitudinal modes can greatly degrade the frequency response of the device.

In addition to being dependent on the length of the cavity, these spurious modes

are also affected by the spaces between the coupled transducer and the gratings and by the periodicity of the coupled gratings and of the coupled transducer. There is no simple way to predict these longitudinal mode responses. They can only be analyzed using a computer model to calculate the frequency response.

A desired frequency response can be achieved by adjusting these parameters. For example, for a given grating and transducer length and a given grating period, the period of the coupled transducer and the spaces between the gratings and transducer can be tuned in the simulation to get the desired design. This iterative process permits the suppression of the spurious longitudinal modes.

In addition to the spurious longitudinal modes, the higher order transversal mode responses can also degrade the frequency response of the WGC resonator. Since the higher order transversal modes have a higher phase velocity, the resonant frequencies for these modes appear at the high end of the filter response. The existence of higher order modes depends on the guiding effect of the coupled structure. For a given aperture, if the film is very thick, then the velocity difference between the grating region and the metallization region is larger and more transverse modes will be supported in the waveguide structure. Reducing the film thickness to suppress these transverse modes will increase the length of the reflector gratings. It is also possible to reduce the aperture so that only the two desired transverse modes are supported, but this will lower the IDT radiation.

4.5 Simulation and Experimental Results

The frequency response of the WGC resonators can be computed from the procedure described above using the COM models for the coupled gratings, coupled transducers and the two-track acoustic transmission lines. In the analysis, the admittance matrix can be computed over the frequency range of interest. The electrical characteristics and the operation the device can be analyzed from these parameters. The response of two waveguide coupled resonators will now be analyzed and compared with the experimental results.

The configuration of the typical two-pole device is shown in Figure 4.1. Our discussion will centre around two devices with design parameters given in Table 1.

Table 1. Design parameters of the waveguide coupled resonators

	Device 1	Device 2
Substrate	ST-X Quartz	
Electrodes	Aluminum	
Film thickness	6000 Å	8000 Å
IDT period (Λ_T)	15.79 μm	15.71 μm
Grating period (Λ_G)	15.79 μm	15.79 μm
IDT overlap ($W/(2\Lambda_G)$)	12	12
Coupling gap ($W/(2\Lambda_G)$)	1.5	1.5
IDT length	301 fingers	301 fingers
Reflectors (per side)	200 strips	200 strips

The designs use the finger-in-phase [19] approach. In the absence of electrical feedthrough, the frequency responses for the finger-in-phase and finger-out-of-phase

designs are the same. However, electrical feedthrough, which can be treated as a bridge capacitor [19, 25] between the two ports of the WGC resonator, causes the in-phase alternative to have a slightly higher out-of-band rejection because the feedthrough signal is out-of-phase with the weak spurious mode responses. The choice also affects the generation of transverse modes. If the voltages applied to the two IDTs are the same, the symmetric modes are excited in the finger-out-of-phase design while the anti-symmetric modes are excited in the finger-in-phase type. On the other hand, if the voltages applied to the two IDTs are opposite, the anti-symmetric modes and symmetric modes are excited for the finger-out-of-phase and finger-in-phase designs, respectively.

These two devices were designed to operate at the nominal frequency of 100 MHz. For illustration purpose, the two devices have very different frequency responses. The first device has a very strong longitudinal mode response which degrades the filtering character of the device. In the second device, the spurious longitudinal mode is suppressed by properly choosing the distances between the coupled gratings and the coupled transducer and the periodicity of both the coupled transducer and gratings. The theoretical results agree well with the experimental results.

4.5.1 Device with spurious longitudinal modes

Figure 4.7(a) gives the Y_{11} parameter of device 1. Its real part is the radiation conductance, while the imaginary part is the sum of the radiation susceptance and the static capacitance of the input IDT. Several peaks are observed on the radiation

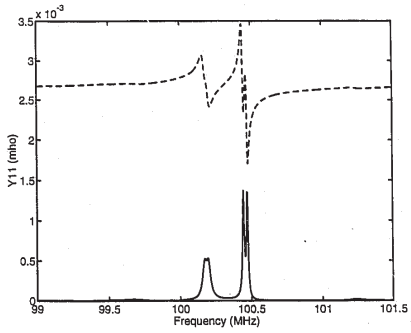

Figure 4.7(a) Simulated input admittance (Y_{11}) of WGC resonator 1

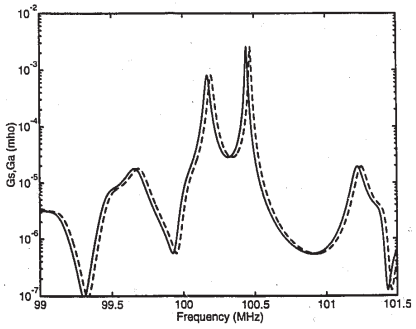

Figure 4.7(b) Simulated radiation conductances for symmetric (solid line) and anti-symmetric mode (dashed line) of WGC resonator 1

conductance curve, which is a measure of the conversion of electrical energy into acoustical energy by the input IDT. These peaks correspond to device resonances and more energy is transmitted to the load at these frequencies. From the plot of the radiation conductance, we can identify the frequencies of the resonant modes and their relative strengths in the device.

We can decompose Y_{11} into symmetric and antisymmetric input admittances by applying equal or opposite voltages to the two IDTs, respectively. Either the resonant mode with symmetric transverse field distribution or the resonant mode with the anti-symmetric transverse field distribution will be excited. The radiation admittances under these driving conditions are the radiation admittances for the transverse symmetric and anti-symmetric modes, respectively. The real parts of these radiation admittances are shown in Figure 4.7(b). We see that the two radiation conductances have the same shape, but are shifted in frequency. The shift is caused by the different phase velocities of the transverse symmetric and anti-symmetric modes. The real part of the Y_{12} has opposite signs at the two resonant frequencies because of the symmetric and anti-symmetric transverse field distribution of two modes.

Figures 4.8(a) and 4.8(b) give the simulated and experimental results, respectively, for the S_{21} parameter of the device. We can see that the simulation result agrees with the measurement. In this device, in addition to the principal longitudinal mode, another longitudinal mode is strongly excited, which greatly degrades the filter characteristics.

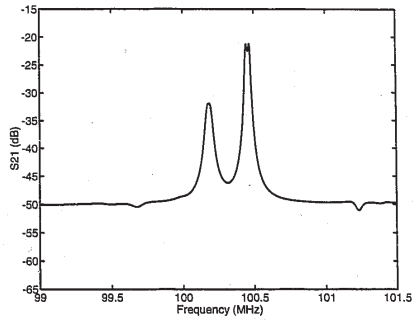

Figure 4.8(a) Simulated S_{21} for WGC resonator 1

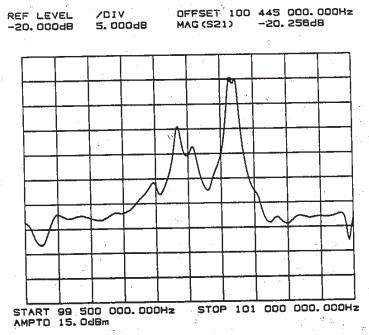

Figure 4.8(b) Measured S_{21} for WGC resonator 1

In practical applications, the spurious longitudinal modes are not desirable. The design of a second device, with parameters given in the second column of Table 1, is optimized to suppress this longitudinal mode and enhance the principal longitudinal mode.

4.5.2 Waveguide coupled resonator with optimized design

In device 2, the period of the IDT is slightly shorter than the period of the reflector gratings so that the electro-acoustical coupling between the transducers and reflector gratings is maximized. This is necessary because finger reflections move the frequency that produces the maximum IDT radiation conductance down from the Bragg frequency of gratings with the same period. The radiation conductance of the coupled transducer is shown in Figure 4.9. We can see that the maximum of the radiation conductance is shifted down by about 0.5 MHz. Therefore, the nominal (synchronous) frequency of the transducer is increased by the same amount to compensate. A second step was taken to suppress the unwanted longitudinal mode. From the frequency response of the device 1, we can see that this mode has a resonant frequency below that of the principal mode. From the curve of the radiation conductance of a coupled transducer, we observe a null at a frequency lower than the maximum of the radiation conductance. By matching the frequency of the unwanted longitudinal mode with that of the null, while maintaining the position of the desired mode, the former will be suppressed because of the lack of excitation. This can be done by changing the distance between the gratings

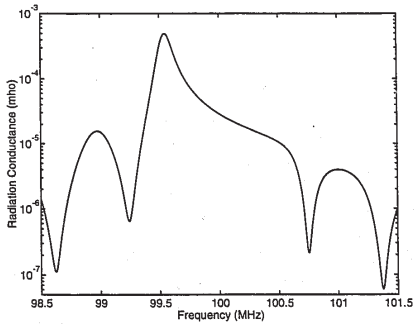

Figure 4.9 Radiation conductance of a coupled transducer

and by changing the length of the coupled transducers.

By iterative simulations, the design parameters were determined. The simulated and measured radiation conductances at one port (real(Y_{11})) are shown in Figure 4.10(a) and (b) respectively. The measured radiation conductance is calculated from measured full two-port S parameters. The simulated and measured S_{21} parameters of the resonator are shown in Figures 4.10(c) and 4.10(d). We can see that the unwanted longitudinal mode is suppressed. The simulated results agree with the experimental results. We also note that, as a result of the optimization in the electro-acoustical coupling, the insertion loss is smaller for device 2 than for device 1.

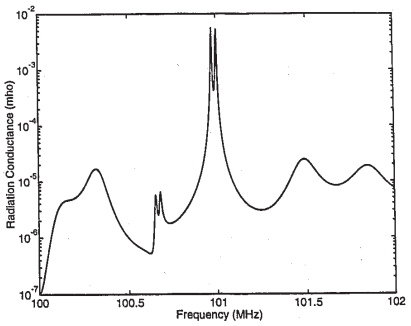

Figure 4.10(a) Simulated radiation conductance for WGC resonator 2

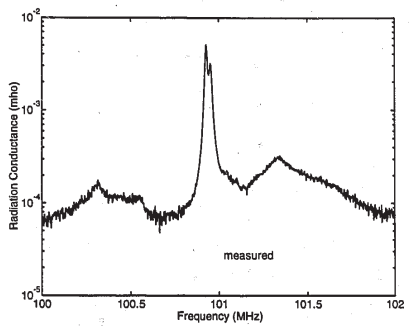

Figure 4.10(b) Measured radiation conductance for WGC resonator 2

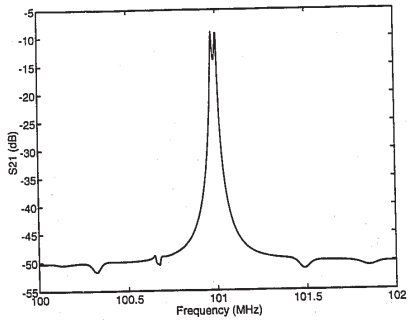

Figure 4.10(c) Simulated S_{21} for WGC resonator 2

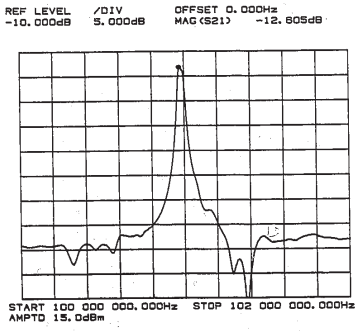

Figure 4.10(d) Measured S_{21} for WGC resonator 2

4.6 Simulations of Four-pole Resonators

The WGC resonators discussed above are two-pole devices. The number of poles in a coupled resonator is equal to the number of resonant modes. The steepness of the transition band of the frequency response can be increased by using more poles in the coupled resonator. One way to increase the number of the resonant cavities is to increase the number of parallel tracks in the two-pole WGC resonator [29]. The other way, proposed by the author[27], is to put another two resonant cavities in the longitudinal direction. The resulting device is a four-pole coupled resonator with both waveguide coupling and longitudinal coupling. The theory developed in this thesis can be applied to the analysis of these devices.

4.6.1 Four-track WGC Resonator

The number of tracks in a waveguide coupled resonator can be increased to produce a device with more than two poles. Recently, a four-track device of this type was reported [29]. The structure of a four-track WGC resonator is shown in Figure 4.11(a), with four IDTs serving as four electrical ports. The admittance matrix for the four-port network is a 4 × 4 matrix, though two-port devices with this structure can be obtained by various topological connections. The theory developed in this thesis for coupled transducers and coupled gratings can be easily extended to model these multi-track coupled transducers and coupled gratings.

In addition to the coupling of counter-propagating waves on the same track, the

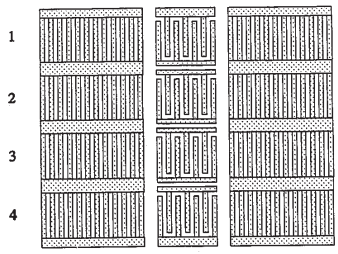

Figure 4.11(a) Four-track WGC resonator structure

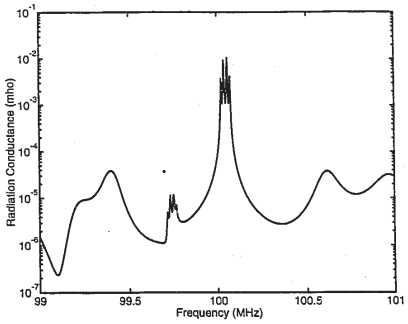

Figure 4.11(b) Simulated radiation conductance at port 1

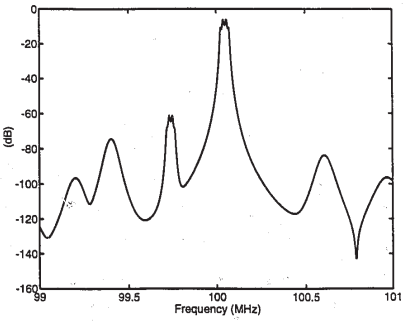

Figure 4.11(c) Simulated scattering parameter S_{41}

coupling of waves travelling in the same direction on adjacent tracks is assumed to occur. The COM equation for multi-track coupled transducers and coupled gratings can be obtained in a very similar way as that for the two-track case. For the four-track case, the coupling matrix C is expressed as

$$C = \begin{bmatrix} -j\delta & j\kappa & j\mu & 0 & 0 & 0 & 0 & 0 \\ -j\kappa^* & j\delta & 0 & -j\mu^* & 0 & 0 & 0 & 0 \\ j\mu^* & 0 & -j\delta & j\kappa & j\mu & 0 & 0 & 0 \\ 0 & -j\mu & -j\kappa^* & j\delta & 0 & -j\mu^* & 0 & 0 \\ 0 & 0 & j\mu^* & 0 & -j\delta & j\kappa & j\mu & 0 \\ 0 & 0 & 0 & -j\mu & -j\kappa^* & j\delta & 0 & -j\mu^* \\ 0 & 0 & 0 & 0 & j\mu^* & 0 & -j\delta & j\kappa \\ 0 & 0 & 0 & 0 & 0 & -j\mu & -j\kappa^* & j\delta \end{bmatrix} \quad (4.19)$$

The COM equations for the four-track gratings and transducers can be written in the same form as those for the two-track ones in chapter 2. The solutions of these COM equations also have the same form as those for two-track devices.

The equations for the currents can be written in the same form as in the two-track case. The current for each track is assumed to be only affected by the waves on that track and by the voltage applied to that track.

As an example, Figure 4.11(b) shows the simulated input radiation conductance of a four-track device. Figure 4.11(c) shows the simulated frequency response of S_{41}. As expected, we see that the response contains four resonant peaks in the main passband, corresponding to the four transverse modes.

4.6.2 Waveguide and longitudinally coupled resonator

The in-line coupled resonator in Figure 1.7(a) has two resonant cavities that share a common semi-transparent reflector grating. The coupling is controlled by varying the length of the grating between the cavities. It has been established [13] that two gratings separated by a quarter wavelength form a high Q resonator with the resonant frequency ideally centred at the Bragg frequency. Therefore two resonant cavities can be added to the structure by placing a coupled grating, separated by a quarter wavelength, at one end of the two-track WGC resonator. The structure is shown in Figure 4.12. It is expected that this will produce a device with four poles.

In the simulation, it is assumed that a 100 MHz device has 150.5 finger pairs in the coupled transducer. The finger reflection within the transducer is assumed to be zero. This can be realized by using split fingers. There are 200 reflector strips in the two gratings at the far ends and there are 160 reflector strips in the centre gratings. The space between the transducer and gratings is 0.75 Λ. The aperture of each track is assumed to be 20Λ. The coupling coefficient between the two tracks μ is assumed to be -27 m^{-1}, while the coupling coefficient for reflection κ is -700 m^{-1}.

The real and imaginary parts of the Y_{11} parameter are shown in Figure 4.13(a). We see that there are four resonant peaks in the real part of Y_{11}. Figure 4.13(b) shows the simulation of the Y_{21} parameter of the device. The peaks in the real part of Y_{21} correspond to the peaks at the real part of Y_{11}, but the signs at these modes alternate. This behaviour represents the symmetric and anti-symmetric property of the mode distributions in the

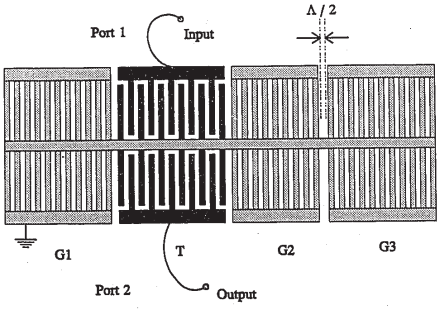

Figure 4.12 The WGC resonator with longitudinal coupling

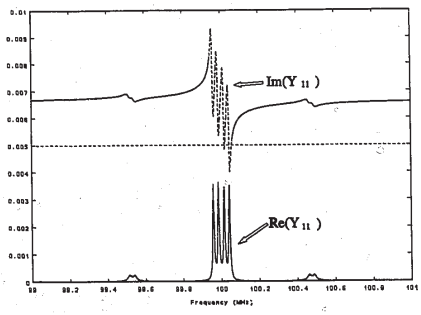

Figure 4.13(a) The Y_{11} of device in Figure 4.12

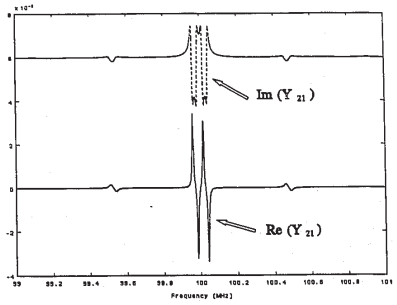

Figure 4.13(b) Y_{21} of the device in Figure 4.12

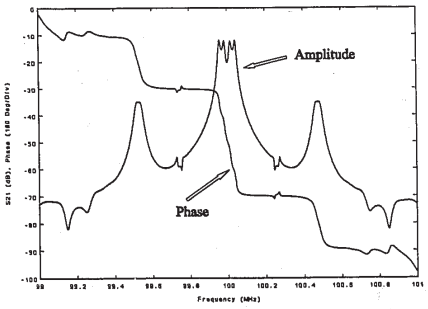

Figure 4.13(c) S_{21} of the device in Figure 4.12

longitudinal and transverse directions. The S_{21} parameter of the unmatched device in a 50 Ω system can be computed from the admittance matrix and is shown in Figure 4.13(c). We see that there are four peaks at the passband.

4.7 Longitudinal Mode Profiles

The longitudinal mode profile of each of the longitudinal resonances is very important in understanding the operation of resonant devices. The COM formalism presented in this thesis has the added benefit of providing a method of directly computing it.

An experimental study of the fundamental longitudinal mode was reported by Hunt *et al* [21], but no theory for the longitudinal mode profiles has yet appeared in the public literature.

The COM theory for coupled gratings and coupled IDTs developed in this thesis describes the wave propagation in the longitudinal direction. The longitudinal mode profile at each resonant frequency can therefore be calculated by applying appropriate boundary conditions. The transmission matrix notation for the COM equations is especially well suited to such calculations, since the complex amplitude of the waves can be calculated directly.

From equation (2.39), the longitudinal distribution of waves in a reflector grating can be expressed by the transmission relation,

From equation (2.45), the longitudinal distribution of waves in the coupled

$$w(x) = VE(x)V^{-1}w(0) \tag{4.20}$$

transducer is expressed as,

$$w(x) = VE(x)V^{-1}\,w(0) + (VE(x)V^{-1}-I)C^{-1}f \tag{4.21}$$

The wave amplitude vector W_2 at the coupled transducer edge is known from the computation of the admittance matrix. Therefore, the wave amplitude vectors within the coupled gratings and transducers can be calculated from W_2 by choosing the edges of the gratings or transducers as reference point $x = 0$.

As an example, consider a third device. It has 300.5 finger pairs in the coupled IDTs and 300 reflectors in the coupled reflector gratings. The finger periodicity of the gratings and IDT are the same and corresponds to a Bragg frequency of 280 MHz. The distance between the gratings and IDTs is 0.75 Λ. The film thickness is about 2% of the wavelength [19]. From the radiation conductance of the resonator, we can identify the resonant frequency of each of the longitudinal modes. In Figure 4.14(a), for example, the first longitudinal mode f_{1s} is located at 280.06 MHz, and the second longitudinal mode f_{2a} at 279.81 MHz and the third longitudinal mode f_{3s} at 279.05 MHz.

Figure 4.14(b) shows the amplitude distributions of the standing waves for the above three longitudinal modes. For each pair of transverse modes, the longitudinal mode profiles are the same. For example, the longitudinal mode profile for mode f_{2a} is the same as that for f_{2s}. The result is obtained by calculating the value of the waves at equally spaced points in the device at the resonant frequency of each of the modes. We see the characteristic number of half-cycle variations within the cavity, with an exponential decay

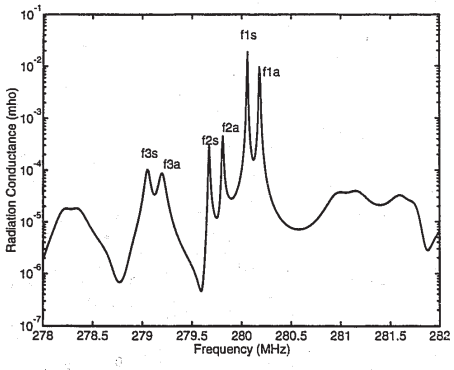

Figure 4.14(a) Simulated radiation conductance at one port

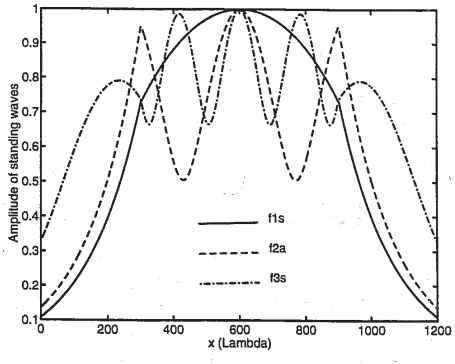

Figure 4.14(b) Computed longitudinal mode profiles for the first three modes

into the end reflector arrays. The lowest mode has the highest confinement of energy in the longitudinal direction. The third order mode is less confined than the second and first order modes.

4.8 COM Parameters

Thus far, the theory of coupling-of-modes and its application to the analysis of SAW resonators has been discussed. It has been shown that the properties of the gratings and of the IDTs can be easily expressed by the COM equations. The determination of the COM parameters has, however, not been addressed.

The COM parameters for single track devices are the reflection coefficient κ and transduction coefficient α. For coupled gratings, the coupling coefficient μ between waves travelling in the same direction on adjacent tracks should be added.

The κ and α constants for a single track can be determined by direct measurement [26]. Alternatively, these COM parameters can be estimated theoretically, as was done by Chen and Haus [23]. They combined the COM equations with the variation principle to obtain a theoretical expression for the COM parameters and thereby obtained numerical solutions.

For coupled gratings, we assume that the reflection coefficient κ and the transduction coefficient α will be the same as for single track gratings and IDTs. The remaining parameter, μ, can be determined from equation (2.38) which describes its relation to the frequency splitting. The frequency difference between the two transverse modes can be obtained from references [19, 20].

4.9 Conclusions

In this chapter we have discussed the modelling of waveguide-coupled resonators using the COM theory. The device properties can be expressed in terms of the *Y*-parameters for a two-port network. The admittance matrix can be obtained over the frequency range of interest by finding the COM solution for gratings and transducer after applying the boundary conditions at the section boundaries and at the ends of the device. The *S*-parameters for the device can be calculated from the corresponding admittance matrix.

The design optimization of the waveguide-coupled resonator is discussed. It is shown that maximum electrical coupling can be obtained by shifting the synchronous frequency of the IDTs to make the maximum radiation conductance equal to the Bragg frequency of the gratings. Further, a spurious longitudinal mode response can be minimized by placing the null of the radiation conductance at the undesired longitudinal mode frequency. The theoretical results agree well with the experiments.

In addition to the two-pole WGC resonators, the modelling of a four-track waveguide resonator with four poles and of a four-pole resonator with both waveguide coupling and longitudinal coupling are demonstrated.

The longitudinal mode profile for the waveguide-coupled resonators is calculated using the coupled grating and coupled transducer models.

The coupling coefficient introduced to describe the coupling between waves travelling in the same direction on parallel tracks can obtained from a waveguide analysis.

CHAPTER 5

CONCLUSION

SAW resonators, longitudinally coupled resonators and waveguide coupled resonators have been studies in thesis. Efficient and accurate models for these devices, have been developed based on the coupling-of-modes theory.

In chapter 2, the COM theory for the analyses of the two-port resonators, longitudinally coupled resonators and waveguide coupled resonators are reviewed and developed. The previous coupling-of-modes theory used in the analyses of the SAW devices can only be applied for single-track devices. In these devices, the waves are propagating in single track, such as the case of resonators and longitudinally coupled resonators. In the case of the waveguide coupled resonator, the waves in the devices are propagating in two tracks. The interaction of these waves causes the coupling of waves at the two tracks. In order to model such device, the COM theory need to be extended to include the coupling between the waves in the two tracks. In this thesis, the COM theory for the coupled gratings and coupled transducers with two or more tracks is established. In this theory, the reflection, generation, and coupling of the waves between the two tracks or more tracks are included in the model. Closed-form solutions of the COM equations have been obtained in transmission matrix form, which makes it easy to calculate the effect of cascading the gratings. Using this theory, waveguide coupled resonators can be analyzed.

In chapter 3, the resonators and longitudinally coupled resonators are studied. The operation of the device are discussed using the standing wave pattern analyses. In these devices, the number of resonant modes are mostly affected by the distances between the two IDTs. For resonators, the distance between the IDTs has to be integral number of half wavelength in order to have only one dominant mode. For longitudinally coupled resonators, this distance has to be integer number of half wavelength plus a quarter wavelength in order to have the two longitudinal modes excited and detected equally. The COM model gives full description of the electrical characteristics of these devices. The S parameters can be computed from the admittance matrix obtained from the COM model. The simulation results agree well with the experimental results on different designs of resonators and longitudinally coupled resonators.

In chapter 4, the waveguide coupled resonators are studies. Using the COM theory developed in chapter 2, the electrical characteristics of two-pole WGC resonators can be fully simulated. Optimized design for the waveguide coupled resonator can be achieved using the iterative simulations. Design optimization is demonstrated based on the model established. An procedure for design optimization is given. In the design of waveguide-coupled resonators, methods for the optimization of electrical coupling and for the suppression of the longitudinal modes are proposed. This procedure is demonstrated in the design process of an experimental device. Two devices with different designs are designed, fabrication and compared with the simulations. The simulation results agrees well with the experimental ones. Because of its modular nature in describing the components of the devices, the COM model for waveguide coupled resonator is very

flexible and can be easily applied to other structures, such as the four-track waveguide coupled resonators and the coupled resonators with both longitudinal coupling and waveguide coupling. A four-pole waveguide coupled resonator with four tracks and a four-pole coupled resonator with both waveguide coupling and longitudinal coupling are analyzed using the COM model. In addition to the electrical characteristics, the longitudinal filed distributions of the waves within the devices can be computed using the COM theory. The longitudinal filed distributions of the acoustic waves are calculated at the three resonant frequencies.

SAW longitudinally coupled resonators and waveguide coupled resonators have been gained dramatically wide applications in the wireless communication systems. The models for these devices are very important and very useful for SAW designers and system users in designing process of the devices and system. In addition to the modelling of theses devices, the operation principles of the these devices are also studied. In this respect, a better understanding of operation of these devices will help SAW designers to design devices more efficiently and properly.

APPENDIX A

THE SOLUTION OF THE COM EQUATIONS

The COM equations for reflection gratings, IDTs, coupled gratings and coupled transducers in this thesis can be written in a general form as following,

$$\frac{dw}{dx} = Cw + f \tag{A.1}$$

where $w(x)$ is a 1×2 or 1×4 vector for single track and two-track elements, respectively, which is given in equations (2.11) and (2.36). C is the 2×2 or 4×4 matrix which is defined in equations (2.11) and (2.36) for the different cases. f is a 1×2 or 1×4 vector associated with the applied voltages. The definitions are given in equations (2.20) and (2.46). For uniform gratings and transducers, the elements of C and f are independent of x. The solution of COM equation can be expressed in the same form for single-track gratings and IDTs as multi-track ones. In the following derivation, the gratings and transducer are assumed to be two-track ones.

A general solution for equation (A.1) can be expressed as

$$w = V_m \begin{bmatrix} e^{\lambda_1 x} & 0 & 0 & 0 \\ 0 & e^{\lambda_2 x} & 0 & 0 \\ 0 & 0 & e^{\lambda_3 x} & 0 \\ 0 & 0 & 0 & e^{\lambda_4 x} \end{bmatrix} a + b \tag{A.2}$$

where a and b are 1×4 vectors independent of x. V_m is the 4×4 eigenvector matrix for matrix C. λ_i ($i = 1, 4$) are the eigenvalues for matrix C.

The first part of the solution is the solution for the homogenous equation

$$\frac{dw}{dx} = Cw \tag{A.3}$$

which is equation (A.1) for the case of $f = 0$.

Substituting (A.2) into (A.1), we have

$$Cb + f = 0 \tag{A.4}$$

Therefore, vector b is obtained,

$$b = -C^{-1}f \tag{A.5}$$

Where C^{-1} is the inverse of matrix C.

If the value of wave amplitude vector $w(x)$ at $x = 0$ is $w(0)$, then

$$w(0) = V_m \begin{bmatrix} 1 & 0 & 0 & 0 \\ 0 & 1 & 0 & 0 \\ 0 & 0 & 1 & 0 \\ 0 & 0 & 0 & 1 \end{bmatrix} a + b = V_m a - C^{-1}f \tag{A.6}$$

From (A.6), vector a can be obtained.

$$a = V_m^{-1}(w(0) - b) \tag{A.7}$$

From (A.7), (A.5) and (A.2), $w(x)$ can be expressed as,

$$\begin{aligned} w(x) &= V_m E(x) V_m^{-1}(w(0) - b) + b \\ &= V_m E(x) V_m^{-1} w(0) + [\, V_m E(x) V_m^{-1} - I_m \,] C^{-1} f \end{aligned} \tag{A.8}$$

where I_m is the 4×4 unit matrix. $E(x)$ is defined by

$$E(x) = \begin{bmatrix} e^{\lambda_1 x} & 0 & 0 & 0 \\ 0 & e^{\lambda_2 x} & 0 & 0 \\ 0 & 0 & e^{\lambda_3 x} & 0 \\ 0 & 0 & 0 & e^{\lambda_4 x} \end{bmatrix} \tag{A.9}$$

The solution for the current in the transducers and coupled transducers can be obtained from the solution of the wave amplitudes $w(x)$. The solution of the current for single track gratings and IDTs can be expressed in the same form as for the two-track ones. Here we derive the solution for the two-track case.

The spacial differentiation of the two currents I_1 and I_2 are expressed in equation (2.44) as,

$$\begin{aligned} \frac{dI_1}{dx} &= -2j\alpha^* w^{*(1)} - 2j\alpha w^{-(1)} + j\omega C_o V_1 \\ \frac{dI_2}{dx} &= -2j\alpha^* w^{*(2)} - 2j\alpha w^{-(2)} + j\omega C_o V_2 \end{aligned} \tag{A.10}$$

These equations can be written in matrix form as,

$$\frac{d}{dx}\begin{bmatrix} I_1 \\ I_2 \end{bmatrix} = Nw + j\omega C_o \begin{bmatrix} V_1 \\ V_2 \end{bmatrix} \tag{A.11}$$

where N is a 2×4 matrix defined by

$$N = \begin{bmatrix} -2j\alpha^* & -2j\alpha & 0 & 0 \\ 0 & 0 & -2j\alpha^* & -2j\alpha \end{bmatrix} \tag{A.12}$$

Substituting the solution of $w(x)$ from (A.2), (A.11) can be expressed as

$$\frac{d}{dx}\begin{bmatrix} I_1 \\ I_2 \end{bmatrix} = N(V_m E(x)a + b) + j\omega C_o \begin{bmatrix} V_1 \\ V_2 \end{bmatrix} \tag{A.13}$$

By integrating the equation from $x = 0$ to $x = L_T$, the currents I_1 and I_2 can be obtained.

We first look at the integration of $E(x)$. The integration of $E(x)$ can be expressed as

$$\int_0^{L_T} E(x)\,dx = \Lambda_m^{-1}(E(L_T) - I_m) \tag{A.14}$$

where Λ_m is a 4×4 matrix

$$\Lambda_m = \begin{bmatrix} \lambda_1 & 0 & 0 & 0 \\ 0 & \lambda_2 & 0 & 0 \\ 0 & 0 & \lambda_3 & 0 \\ 0 & 0 & 0 & \lambda_4 \end{bmatrix} \tag{A.15}$$

The currents can be expressed as

$$\begin{aligned} \begin{bmatrix} I_1 \\ I_2 \end{bmatrix} &= \int_0^{L_T} \left(N(V_m E(x)a + b) + j\omega C_o \begin{bmatrix} V_1 \\ V_2 \end{bmatrix} \right) dx \\ &= N[V_m \Lambda_m^{-1}(E(L_T) - I_m)a + bL_T] + j\omega C_T \begin{bmatrix} V_1 \\ V_2 \end{bmatrix} \\ &= N[V_m \Lambda_m^{-1}(E(L_T) - I_m)V_m^{-1}(w(0) - b) + bL_T] + j\omega C_T \begin{bmatrix} V_1 \\ V_2 \end{bmatrix} \\ &= N[V_m \Lambda_m^{-1}(E(L_T) - I_m)V_m^{-1}w(0) \\ &\quad + (I_m L_T - V_m \Lambda_m (E(L_T) - I_m)V_m^{-1})b] + j\omega C_T \begin{bmatrix} V_1 \\ V_2 \end{bmatrix} \\ &= NV_m \Lambda_m^{-1}(E(L_T) - I_m)V_m^{-1}w(0) \\ &\quad + N(V_m \Lambda_m^{-1}(E(L_T) - I_m)V_m^{-1} - I_m L_T)C^{-1}f + j\omega C_T \begin{bmatrix} V_1 \\ V_2 \end{bmatrix} \end{aligned} \tag{A.16}$$

where $C_T = C_o L_T$, which is the static capacitance of the transducer.

APPENDIX B

THE FABRICATION OF THE DEVICES

All the experimental devices discussed in this thesis were fabricated at the Microwave Acoustics Laboratory, McMaster University. The limitation of the equipments restrict the attainable line-width to about 8 μm in the fabrication. This corresponds to about 100 MHz of the single finger IDT operating frequency on $LiNbO_3$ and ST-X Quartz. Therefore, in this thesis, the operating frequencies of the devices are designed at 80 to 100 MHz. This is a compromise between the device size and line-width. The line-width of the IDT and grating is a quarter wavelength of the surface acoustic wave at the frequency of IDT midland or the Bragg frequency of the reflection grating. After the design parameters are chosen, the fabrication of the devices is in the following steps.

(1) The making of the photomask

Graphics of 100 times of the desired photomask are plotted on the semi-transparent paper with black ink using a computer controlled plotter. These plots are first reduced to films by 5 times on a camera. Then the developed film mask is reduced by another 20 times on another camera to a glass plates. These masks will be used in the lithographic process for generating the pattern on the photoresist.

(2) The deposition of Aluminum film on the substrate

The wafers for SAW devices such as $LiNbO_3$, and Quartz are cut into small substrates for single device on high speed saw. Then the substrate is cleaned using water, detergent, methanol, acetone on a spinner which hold the substrate. After baked on the oven at about 85°C for 30 minutes, these substrates are put onto the substrate holder in the chamber of the vacuum unit. Aluminum is put in the filament inside the chamber. After the vacuum is pumped down to 1×10^{-5} Torr, the filament is heated to evaporate the aluminum onto the substrates. The film thickness is monitored by the reading of the oscillator with a sensor inside the chamber. After 2 hours, the cooled substrates coated with Aluminum film are taken out of the chamber and ready for the next step.

(3) The lithography

Now the substrates are coated with Aluminum film at the polished side. Then photoresist of the type AZ1350B is coated on top the Aluminum with high speed spinner. The substrates coated with photoresist are baked in oven for 30 minutes. Then the pattern of the photomask is transferred to the photoresist film by exposing to ultraviolet using the mask aligner after. The part of photoresist exposed to ultraviolet is dissolved during the development. The masked part of the photoresist remains on the substrate which will protect the Aluminum under neath from the etchant. Then the developed substrate with the photoresist pattern on it is put into the etchant. The exposed part of the aluminum will

be removed. The Aluminum pattern coated with photoresist is the device obtained. The remained photoresist is dissolved and rinsed with acetone. Then the device with the Aluminum pattern of the mask is on the substrate.

At last, the finished device adhered on the device holder, and the pads are connected to the connectors and measured with network analyzer of 50 Ω system.

REFERENCES

[1] Lord Rayleigh, "On waves propagating along the plane surface of an elastic solid," *Proc. London Math. Soc.*, pp. 4-11, November 1885

[2] R.M. White and F.W. Voltmer, "Direct piezoelectric coupling to surface elastic waves," *Appl. Phys. Lett.*, vol. 7, pp. 314-316, Dec. 1965

[3] D.P. Morgan, *Surface-Wave Devices for Signal Processing*, Elsevier Sciences Publishers B.V., 1985

[4] K. Yamanouchi, H. Odagawa, T. Meguro, Y. Wagatsuma and K. Yamamoto "Nano-meter electrode fabrication technology using anodic oxidation resist and application to 20 GHz range SAW devices", *1993 Ultrasonics Symposium Proceedings*, pp. 1263-1266, 1993

[5] J.C.B. Saw, T.P. Cameron, and M.S. Suthers, "Impact of SAW technology on digital microwave radio," *1993 Ultrasonics Symposium Proceedings*, pp. 59-66, 1993

[6] R.C. Rosenfeld, C.S. Hartman and R.B. Brown, "Low-loss unidirectional SAW filters," *Proceedings of 28th Frequency control symposium*, pp. 299-303, 1974

[7] K. Yamanouchi, F.M. Nyffeler and K. Shibayama, "Low insertion loss acoustic surface wave filter using group-type unidirectional transducer," *1975 Ultrasonics Symposium Proceedings*, pp. 317-321, 1975

[8] C.S. Hartmann, P.V. Wright, R.J. Kansy and E.M. Garber, "An analysis of SAW IDTs with internal reflections and the application of the design to single phase unidirectional transducers," *1982 Ultrasonics Symposium Proceedings*, pp. 40-46, 1982

[9] M.F. Lewis, "Low-loss SAW devices employing single stage fabrication", *1983 Ultrasonics Symposium Proceedings*, pp. 104-108, 1983

[10] K. Yamanouchi and H. Furuyashiki, "Low-loss SAW filter using internal reflection types of new single-phase unidirectional transducers," *1984 Ultrasonics Symposium Proceedings*, pp. 68-71, 1984

[11] C.K. Campbell and C.B. Saw, "Analysis and design of low-loss SAW filters using single-phase unidirectional transducers," *IEEE Trans. on Ultrasonics, Ferroelectric, and Frequency Control*, vol. 34, no. 3, pp. 357-367, 1987

[12] E.J. Staples, J.S. Schoenwald, R.C. Rosenfeld and C.S. Hartmann, "UHF surface acoustic wave resonators," 1974 Ultrasonics Symposium Proceedings, pp. 245-252, 1974

[13] P.S. Cross and R.V. Schmidt, "Coupled surface-acoustic-wave resonators," *Bell System Technical Journal*, vol. 56, no. 8, pp. 1447-1482, October 1977

[14] L.A. Coldernand and R.L. Rosenberg, " SAW resonator filters overview: Design and performance tradeoffs," *1978 Ultrasonics Symposium Proceedings*, pp. 422-432, 1978

[15] L.A. Coldernand, R.L. Rosenberg, and Rentschler, "Monolithic transversely coupled SAW resonator filters," *1977 Ultrasonics Symposium Proceedings*, pp. 888-893, 1977

[16] H.F. Tiersten and R.C. Smythe, "Guided acoustic-surface-wave filters," *1975 Ultrasonics Symposium Proceedings*, pp. 293-294, 1975

[17] E.J. Staples, and R.C. Smythe, "SAW resonators and coupled resonator filters". *1976 Frequency Control Proceedings*, pp. 322-327, 1976

[18] L.A. Coldern, "Coupled slot waveguide SAW resonators," *Electronics Letters*, vol. 13, no. 19, pp. 559-561, November 1977.

[19] M. Tanaka, T. Morita, K. Ono and Y. Nakazawa, "Narrow bandpass filter using double-mode SAW resonators on Quartz," *38th Annual Frequency Control Symposium*, pp.286-293, 1984

[20] W.D. Hunt, T. Cameron, J.C.B. Saw, Y. Kim and M.S. Suthers, "Mode profiles in waveguide-coupled resonators," *Journal of Applied Physics*, vol. 74, no. 8, pp. 4886-4893, 1993

[21] W.D. Hunt, T. Cameron, J.C.B. Saw, Y. Kim and M.S. Suthers, "Transverse and longitudinal modes in waveguide-coupled resonators," *1993 IEEE MTT-S Digest*, pp. 1509-1512, 1993

[22] C.S. Hartmann, P.V. Wright, R.J. Kansy and E.M. Garber, "An analysis of SAW interdigital transducers with internal reflections and the application to the design of single-phase unidirectional transducers," *1982 Ultrasonics Symposium Proceedings*, pp. 40-45, 1982

[23] D.P. Chen and H.A. Haus, "Analysis of metal-strip SAW gratings and transducers," *IEEE Transactions on Sonics and Ultrasonics*, vol. 32, no. 3, pp. 395-408, May 1985

[24] C.K. Campbell, P.M. Smith and P.J. Edmonson, "Aspects of modelling the frequency response of a two-port waveguide-coupled SAW resonator-filter," *IEEE Transactions on Ultrasonics, Ferroelectric and Frequency Control*, vol. 39, no. 6, pp. 768-773, November 1992

[25] C.S. Hartmann, D.P. Chen and J. Heighway, "Modelling of SAW transversely coupled resonator filters using coupling-of-modes modelling technique," *1992 Ultrasonics Symposium Proceedings*, Tucson, AZ, pp. 39-43, 1992

[26] C.S. Hartmann, D.P. Chen and J. Heighway, "Experimental determination of COM parameters for SAW transversely coupled resonator filters," *1992 Ultrasonics Symposium Proceedings*, Tucson, AZ, pp. 211-214, 1992

[27] Y. Xu and P.M. Smith, "Modelling of waveguide-coupled SAW resonators," *IEEE Trans. on Ultrasonics, Ferroelectric and Frequency Control*. vol. 41, no. 2, pp. 256-260, 1994

[28] Y. Xu and P.M. Smith, "A COM analysis of SAW waveguide-coupled resonator filters," *1993 Ultrasonics Symposium Proceedings*, pp. 31-34, 1993

[29] G. Martin, B. Wall, R. Kunze and M. Weihnacht, "Four modes waveguide resonator filters", *1993 Ultrasonics Symposium Proceedings*, pp. 35-39, 1993

[30] J.R. Pierce, "Coupling of modes of propagation," *Journal of Applied Physics*, vol. 25, no. 2, pp. 179-183, February 1954

[31] H. Kogelnik, "Coupled wave theory for thick hologram gratings," *Bell System Technical Journal*, vol. 48, no. 9, pp. 2909-2947, November 1969

[32] H. Kogelnik and C.V. Shank, "Coupled-wave theory of distributed feedback lasers," *Journal of Applied Physics*, vol. 43, no. 5, pp. 2327-2335, May 1972

[33] A. Yariv, "Coupled-mode theory for guided-wave optics," *IEEE Journal of Quantum Electronics*, vol. 9, no. 9, pp. 919-933, September 1973

[34] H.A. Haus, "Grating-filter transformation chart", *Electronics Letters*, vol. 11, pp. 553-554, 1975

[35] H.A. Haus, *Waves and Fields in Optoelectronics*, pp. 217-220, Prentice-Hall, Inc., 1984.

[36] G. Scholl, A. Christ, W. Ruile, P. Russer and R. Weigel, "Efficient analysis tool for coupled-SAW-resonator filters", *IEEE Trans. on Ultrasonics, Ferroelectrics and Frequency Control*, vol. 38, no. 3, pp. 243-251, 1991

[37] B.P. Abbot, *A coupling-of-modes model for SAW transducers with arbitary reflectivity weighting*, Ph.D Dissertation, University of Central Florida, Orlando, Florida, 1989

[38] A. Yariv, *Optical Electronics*, pp. 529-536, Saunders College Publishing, 1991

[39] T. Morita, Y. Watanabe, M. Tanaka and Y. Nakazawa, "Wideband low loss double mode SAW filters," *1992 Ultrasonics Symposium Proceedings*, pp. 95-104, 1992

[40] D.M. Pozar, *Microwave Engineering*, Addison-Wesley Publishing Company, Inc., 1990

[41] C.K. Campbell, *Surface acoustic wave devices and their signal processing applications*, Academic Press, Inc., San Diego, CA, 1989

[42] P.S. Cross, W.R. Shreve and T.S. Tan, "Synchronous IDT SAW resoantors with Q above 10,000", *1979 Ultrasonics Symposium Proceedings*, pp. 824-829, 1979

[43] W.R. Smith, H.M. Gerard, J.H. Collins, T.M. Reeder, and H.J. Shaw, "Analysis of interdigital surface acoustic wave transducers by use of an equivalent circuit model," *IEEE Trans. Microwave Theory and Technology*, Vol. 17, pp. 856-864, November 1969

[44] P.V Wright, "A review of SAW resonator filter technology," *1992 Ultrasonics Symposium Proceedings*, pp. 29-38, 1992

[45] Y. Nakazawa, K.Ono, M. Tanaka, T. Morita and T. Kurosaki, "High frequency narrow band multi-mode filter," U.S. Patent Number: 4,542,356, 1985